In: Atmospheric Turbulence, Meteorological Modeling... ISBN 978-1-60741-091-1
Editors: P. R. Lang and F. S. Lombargo, pp.167-204

Chapter 4

TURBULENCE, TURBULENT MIXING AND DIFFUSION IN SHALLOW-WATER ESTUARIES

Hubert Chanson[1]* and Mark Trevethan[2]
[1]The University of Queensland, Brisbane, Australia
[2]MARUM, The University of Bremen, Germany (formerly Ph.D. graduate in Civil Engineering. The University of Queensland, Brisbane Australia)

1. INTRODUCTION

In natural waterways and estuaries, an understanding of turbulent mixing is critical to the knowledge of sediment transport, storm-water runoff during flood events, and release of nutrient-rich wastewater into ecosystems. The predictions of contaminant dispersion in estuaries can rarely be predicted analytically without exhaustive field data for calibration and validation. Why? In natural estuaries, the flow Reynolds number is typically within the range of 10^5 to 10^8 and more. The flow is turbulent, and there is an absence of fundamental understanding of the turbulence structure. Any turbulent flow is characterised by an unpredictable behaviour, a broad spectrum of length and time scales, and its strong mixing properties. In his classical experiment, Osborne REYNOLDS (1842-1912) illustrated this key feature with the rapid mixing of dye of a turbulent flow (REYNOLDS 1883). This is seen in Figure 1 showing the original Reynolds experiment and a modified Reynolds experiment. In turbulent flows, the fluid particles move in very irregular paths, causing an exchange of momentum from one portion of the fluid to another, as shown in Figure 1 where dye is rapidly dispersed in the turbulent flow regime (Re = 2.3 10^3). In natural estuaries, strong momentum exchanges occur and the mixing processes are driven by turbulence. Interestingly Osborne REYNOLDS himself was involved in the modelling of estuaries (REYNOLDS 1887).

Relatively little systematic research was conducted on the turbulence characteristics in natural estuarine systems, in particular in relatively shallow-water systems. Long-duration

* Email: h.chanson@uq.edu.au - Url: http://www.uq.edu.au/~e2hchans/ - Ph.: + 61 7 3365 3516 - Fax: +61 7 3365 4599

studies of turbulent properties at high frequency are extremely limited. Most field measurements were conducted for short periods, or in bursts, sometimes at low frequency: e.g. BOWDEN and FERGUSON (1980), SHIONO and WEST (1987), KAWANISI and YOKOSI (1994), HAM et al. (2001), VOULGARIS and MEYERS (2004). The data lacked spatial and temporal resolution to gain insights into the characteristics of fine-scale turbulence. It is believed that the situation derived partly from some limitation with suitable instrumentation for shallow-water estuaries.

Herein the turbulence characteristics of shallow-water estuaries with semi-diurnal tides are examined. It is shown that turbulence field measurements must be conducted continuously at high frequency for relatively long periods. Detailed field measurements highlight the large fluctuations in all turbulence characteristics during the tidal cycle. While the bulk parameters fluctuate with periods comparable to tidal cycles, the turbulence properties depend upon the instantaneous local flow properties, and the structure and temporal variability of turbulent characteristics are influenced by a variety of mechanisms.

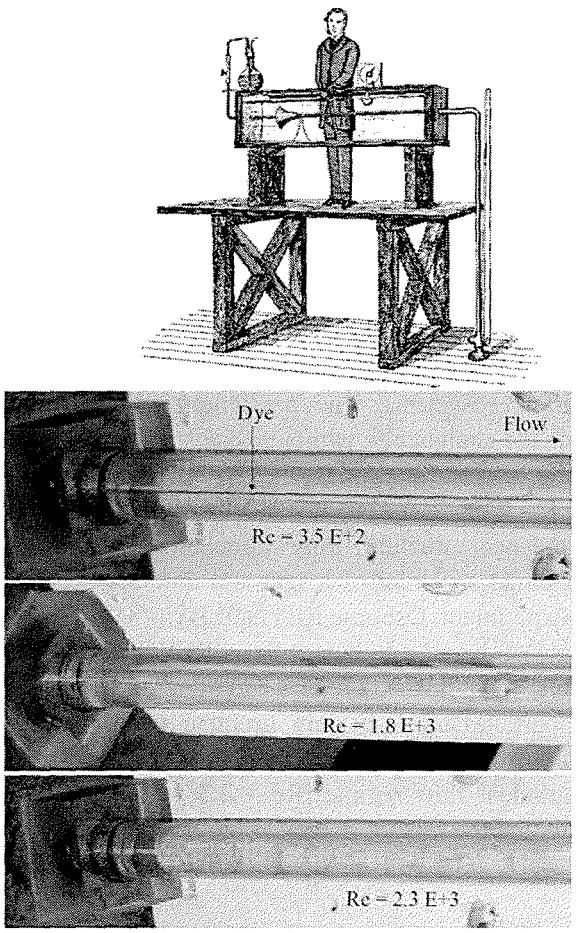

Figure 1. Dye dispersion in laminar and turbulent flows (Left) Gravure of the experimental apparatus of Osborne REYNOLDS (1883) (Right) Dye injection in a circular pipe for Re = 3.5 10^2, 1.8 10^3 and 2.3 10^3

2. TURBULENCE MEASUREMENTS IN SMALL ESTUARIES

2.1. Presentation

Since "turbulence is a three-dimensional time-dependent motion in which vortex stretching causes velocity fluctuations to spread to all wavelengths between a minimum determined by viscous forces and a maximum determined by the boundary conditions of the flow" (BRADSHAW 1971, p. 17), turbulence measurements must be conducted at high frequency to characterise the small eddies and the viscous dissipation process. They must also to be performed over a sampling period significantly larger than the characteristic time of the largest vortical structures to capture the "random" nature of the flow and its deviations from Gaussian statistical properties. Turbulence in natural estuaries is neither homogeneous nor isotropic. Basically detailed turbulence measurements are almost impossible in unsteady estuarine flows unless continuous sampling at high frequency is performed over a full tidal cycle. The estuarine flow conditions and boundary conditions may vary significantly with the falling or rising tide. In shallow-water estuaries and inlets, the shape of the channel cross-section changes drastically with the tides as shown in Figures 2 and 3. Figures 2 and 3 illustrate two sampling sites in a small subtropical estuary at high and low tides. Figure 2 presents the cross-section at the mid-estuary sampling site with more than 3 m depth at high tide and less than 0.6 m of water at low tide. Figure 3 shows a narrower section in the upper estuary at both high and low tides.

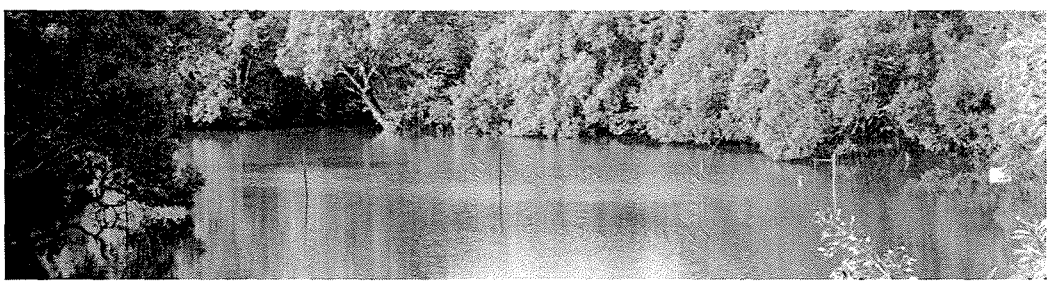

(A) End of flood tide on 16 May 2005 with poles supporting the instrumentation visible across the creek.

(B) Low tide on 23 November 2003 - The water depth was less than 0.6 m in the deepest channel next to the ADV poles during spring tidal conditions.

Figure 2. Sampling site in the mid-estuarine zone of Eprapah Creek, Australia (site 2B, AMTD 2.1 km) looking upstream.

(A) High tide in 28 August 2006 looking downstream (Courtesy of CIVL4120 student Group 3) - The water depth was about 2 m.

(B) Low tide on 8 June 2006 looking upstream (Courtesy of Clive BOOTH).

Figure 3. Sampling site in the upper estuarine zone of Eprapah Creek, Australia (site 3, AMTD 3.1 km).

All these constraints affect the selection of a suitable, rugged instrumentation for field deployment. Traditional propellers and electro-magnetic current meters are adequate for time-averaged velocity measurements and some large-scale turbulence measurements, but these instruments lack temporal and spatial resolution for fine-scale turbulence measurements. Velocity profilers do not work in shallow waters (e.g., less than 0.6 m) while lacking spatial and temporal resolution. A suitable instrumentation for turbulence measurements in shallow-water estuaries is limited to the acoustic Doppler velocimeters (ADV), although the signal can be adversely affected by "spikes", noises and instabilities.

2.2. Turbulence Properties

Turbulent flows have a great mixing potential involving a wide range of eddy length scales (HINZE 1975). Although the turbulence is a "random" process, the small departures from a Gaussian probability distribution constitute some key features. For example, the skewness and kurtosis give some information on the temporal distribution of the turbulent velocity fluctuation around its mean value. A non-zero skewness indicates some degree of temporal asymmetry of the turbulent fluctuation: e.g., acceleration versus deceleration, sweep versus ejection. The skewness retains some sign information and it can be used to extract basic information without ambiguity. An excess kurtosis larger than zero is associated with a peaky signal: e.g., produced by intermittent turbulent events.

In turbulence studies, the measured statistics include usually (a) the spatial distribution of Reynolds stresses, (b) the rates at which the individual Reynolds stresses are produced, destroyed or transported from one point in space to another, (c) the contribution of different sizes of eddy to the Reynolds stresses, and (d) the contribution of different sizes of eddy to the rates mentioned in (b) and to rate at which Reynolds stresses are transferred from one range of eddy size to another (BRADSHAW 1971). The Reynolds stress is a transport effect resulting from turbulent motion induced by velocity fluctuations with its subsequent increase of momentum exchange and of mixing (PIQUET 1999). The turbulent transport is a property of the flow. The turbulent stress tensor, or Reynolds stress tensor, includes the normal and tangential stresses, although there is no fundamental difference between normal stress and tangential stress. For example, $(v_x+v_y)/\sqrt{2}$ is the component of the velocity fluctuation along a line in the xy-plane at 45° to the x-axis; hence its mean square $(v_x^2 + v_y^2 + 2v_x v_y)/2$ is the component of the normal stress over the density in this direction although it is a combination of normal and tangential stresses in the x- and y-axes.

2.3. Field Experiments in Shallow-Water Estuaries with Semi-Diurnal Tides

A series of detailed turbulence field measurements were conducted in two shallow-water estuaries with a semi-diurnal tidal regime (Table 1).

Table 1. - Turbulence field measurements in Australia (Eprapah Creek, QLD) and Japan (Hamana Lake).

Ref.	Dates	Tidal range (m)	ADV system(s)	Sampling rate (Hz)	Sampling duration	Sampling volume
(1)	(2)	(3)	(4)	(5)	(6)	(7)
	Series E					Eprapah Creek, QLD Australia
E1	4/04/03	1.84	10 MHz	25	9 x 25 min	Site 2B, AMTD 2.1 km, 14.2 m from left bank, 0.5 m below surface.
E2	17/07/03	2.03	10 MHz	25	8 hours	Site 2, AMTD 2.0 km, 8.0 m from left bank, 0.5 m below surface.
E3	24/11/03	2.53	10 MHz	25	7 hours	Site 2B, AMTD 2.1 km, 10.7 m from left bank, 0.5 m below surface.
E4	2/09/04	1.81	10 MHz	25	6 & 3 hours	Site 2B, AMTD 2.1 km, 10.7 m from left bank, 0.052 m above bed.
E5	8-9/03/05	2.37	10 MHz	25	25 hours	Site 2B, AMTD 2.1 km, 10.7 m from left bank, 0.095 m above bed.
E6	16-18/05/05	1.36	2 ADVs (10 & 16 MHz)	25	49 hours	Site 2B, AMTD 2.1 km, 10.7 m from left bank, 0.2 & 0.4 m above bed.
E7	5-7/06/06	1.58	2 ADVs (10 & 16 MHz)	25 & 50	50 hours	Site 3, AMTD 3.1 km, 4.2 m from right bank, 0.2 & 0.4 m above bed.
E8	18/06/06	2.10	--	--	12 hours	Sites 1, 2B & 3, AMTD 1.0, 2.1 and 3.1 km
E9	2-4/10/06 & 11-13/10/06	1.89 1.81	--	--	50	Six sampling sites: AMTD 1.0 to 3.4 km
E10	6-8/06/07	1.76	3 ADVs (16 MHz)	50	50 hours	Site 2B, AMTD 2.1 km, 10.7 m from left bank, 0.13 & 0.38 m above bed.
	Series HL					Hamana Lake, Japan
J1	24-25/11/05	0.39	3D-Vector field ADV	32	28 hours	Site 1, 0.25 m above bed, 454 m from left bank.
J2	30/11-1/12/05	0.56	3D-Vector field ADV	32	25 hours	Site 1, 0.25 m above bed, 454 m from left bank.
J3	10-21/12/05	0.6	3D-Vector field ADV	32	30 hours	Site 1, 0.25 m above bed, 454 m from left bank.

Note: AMTD: Adopted Middle Thread Distance measured upstream from the river mouth; Tidal range: maximum tidal range observed at sampling site.

At Eprapah Creek (Australia), the estuarine zone was 3.8 km long, about 1 to 2 m deep mid-stream (Fig. 2 & 3). This was a relatively small estuary with a narrow, elongated and meandering channel (CHANSON et al. 2005, TREVETHAN et al. 2007a, 2008). It is a drowned river valley (coastal plain) type with a small, sporadic freshwater inflow, a cross-section which deepens and widens towards the mouth, and surrounded by extensive mud flats. This type of estuary is very common in Australia. It is also called an alluvial estuary (SAVENIJE 2005) and can be classified as a wet and dry tropical/subtropical estuary (DIGBY et al. 1999). Although the tides are semi-diurnal, the tidal cycles have slightly different periods and amplitudes indicating that a diurnal inequality exists. Table 1 summarises ten field studies conducted between 2003 and 2007. A range of field conditions were tested: tidal conditions from neap tides (Studies E6, E7, E10) to spring tides (Studies E3, E5, E8), and different bathymetry from mid-estuary (Studies E5, E6, E10) to upper estuary (Study E7) (Table 1).

Another series of field studies were undertaken at Hamana Lake, Japan in late 2005 (TREVETHAN 2008). Hamana Lake is a relatively large tidal lake with a small opening to the Pacific Ocean (Fig. 4). It extends approximately 15 km inland and has a surface area of $7.4\ 10^7$ m^2. The width of the entrance is approximately 200 m and is controlled by man made structures (Fig. 4A). The depth of Hamana Lake increases landwards, from less than 1 m near the entrance to more than 12 m further inland. The field investigations were conducted under neap and spring tidal forcing, collecting continuous high frequency turbulence data over a 25 hour period. The sampling site was located in a shallow area near the estuary mouth (Fig. 4). This type of shallow region is typical of restricted entrance (bar-built) type estuaries (DYER 1997). It was located approximately 600 m North-East of the main navigation channel, 450 m South of the nearest bank and approximately 3.5 km NNW of the estuary mouth seen in Figure 4A. The mean depth was approximately 0.9 m during the two field studies and the maximum tidal range during the field studies were 0.39 and 0.56 m.

(A) Estuary mouth in 1999 (Courtesy of Mr. KATO, Omotehama network).

Figure 4. (Continued)

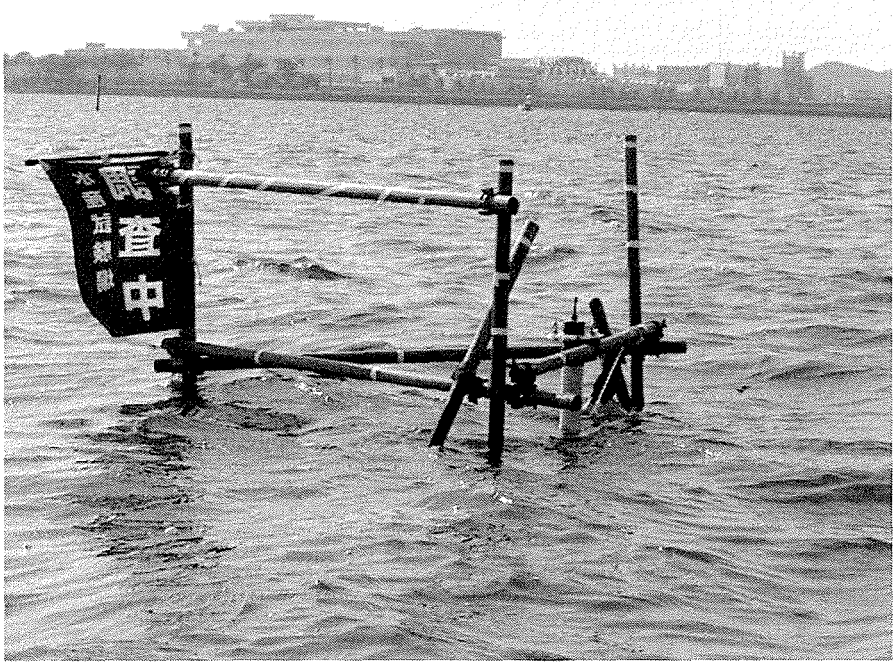

(B) Hamana Lake sampling site on 24 November 2005, looking North to nearest bank about 450 m away.

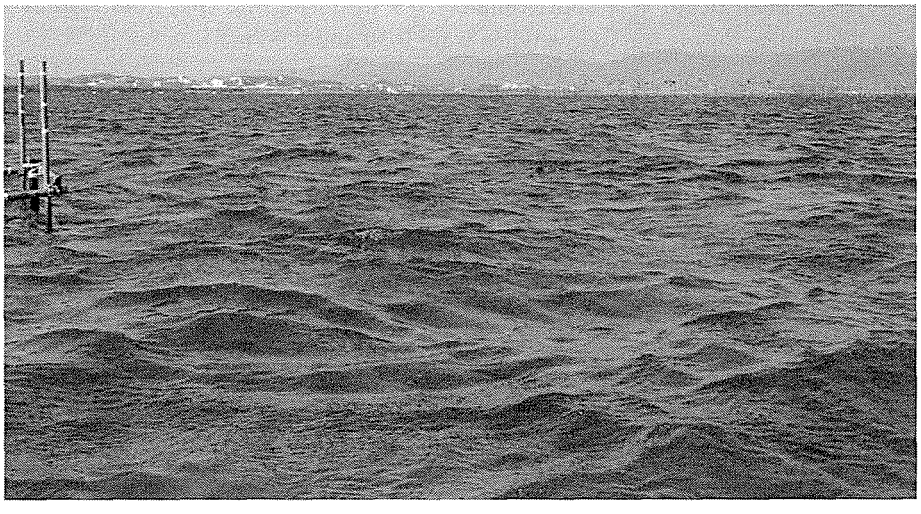

(C) Wind waves on 24 November 2005 with the poles holding the ADV system on the far left.

Figure 4. Photographs of Hamana Lake (Japan).

2.4. Instrumentation

Turbulent velocities were measured with acoustic Doppler velocimetry. That is, a Sontek^{TM} UW 3D ADV (10 MHz) and some Sontek^{TM} 2D micro-ADV (16 MHz) in Australia (Eprapah Creek), and a Nortek^{TM} 3D-Vector field ADV in Japan (Hamana Lake). The turbulent velocity measurements were performed continuously at high frequency for between 8 to 50 hours during various tide conditions (Table 1, columns 5 & 6). All ADV units were synchronised carefully within 20 ms for the entire duration of the studies.

The acoustic backscatter intensity of some ADV signals was also analysed. The backscatter intensity is a function of the ADV signal amplitude that is proportional to the number of particles within the sampling volume :

$$I_b = 10^{-5}\, 10^{0.043\,Ampl} \qquad (1)$$

where the backscatter intensity I_b is dimensionless and the average amplitude Ampl is in counts. (The coefficient 10^{-5} is a value introduced to avoid large values of backscatter intensity.) The backscatter intensity may be used as a proxy for the instantaneous suspended sediment concentration (SSC) within the sampling volume because of the strong relationship between I_b and SSC (THORNE et al. 1991, FUGATE and FRIEDRICHS 2002, CHANSON et al. 2008a). The terms $V_x I_b$ is proportional to the suspended sediment flux per unit area, where V_x is the longitudinal velocity component.

A thorough post-processing technique was developed and applied to remove electronic noise, physical disturbances and Doppler effects (CHANSON et al. 2008b). The field experience demonstrated that the gross ADV signals were unsuitable, and led often to inaccurate time-averaged flow properties and turbulent characteristics. Herein only post-processed data are discussed.

2.5. Calculations of Turbulence Properties

The post-processed data sets included the three instantaneous velocity components V_x, V_y and V_z, and the backscatter intensity I_b, where x is the longitudinal direction positive downstream, y is the transverse direction positive towards the left bank and z is the vertical direction positive upwards. The turbulent fluctuations were defined as : $v = V - \overline{V}$ and $i_b = I_b - \overline{I_b}$, where V was the instantaneous (measured) velocity component, $\overline{V}$ was the variable-interval time average (VITA) velocity and $\overline{I_b}$ was the VITA backscatter intensity. A cut-off frequency was selected with an averaging time greater than the characteristic period of turbulent fluctuations, and smaller than the characteristic period for the time-evolution of the mean tidal properties. An upper limit of the filtered signal was the Nyquist frequency. The selection of the cut-off frequency was derived from a sensitivity analysis (CHANSON et al. 2008b, TREVETHAN 2008). Herein all turbulence data, including the turbulent flux events, were processed using samples that contain 5,000 to 10,000 data points and calculated every 10 s along the entire data sets. In a study of boundary layer flows, FRANSSON et al. (2005) proposed a cut-off frequency that was consistent with the selected sample size.

A basic turbulence analysis yielded the first four statistical moments of each velocity component, the tensor of instantaneous Reynolds stresses, and the statistical moments of the tangential stresses. An auto-correlation analysis yielded further the Eulerian dissipation and integral time scales, τ_E and T_E respectively, for each velocity component (Fig. 5). Herein τ_E was calculated using the method of HALLBACK et al. (1989) extended by FRANSSON et al. (2005) and KOCH and CHANSON (2005).

Note that the turbulence calculations were not conducted when more 20% of the (5,000 to 10,000) sample points within a data sample were corrupted/repaired during the ADV data post-processing.

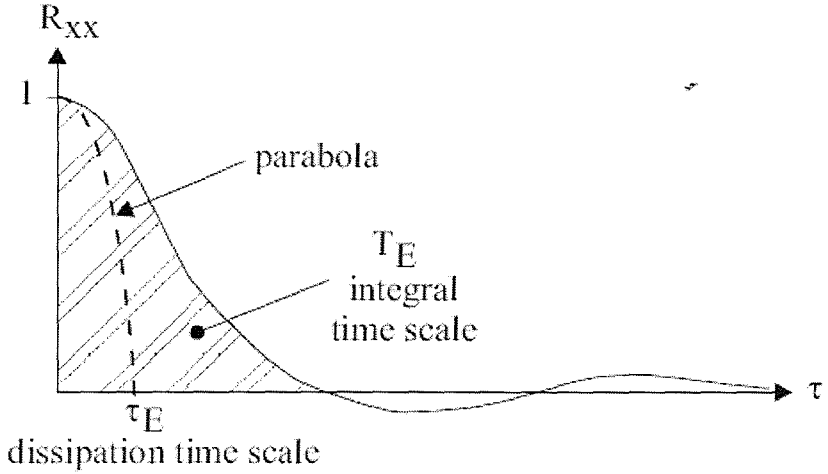

Figure 5. Definition sketch of a velocity component autocorrelation function.

2.6. Turbulent Event Detection Technique

A detection of turbulence bursting events was derived from the technique of NARASIMHA et al. (2007) that was adapted and extended. While this approach differs from more traditional event detection techniques (e.g. JOHANSSON and ALFREDSSON 1982, BAUER et al. 1998, OSTERLUND et al. 2003), it was found to be a robust method well-suited to the study of unsteady estuarine flow (TREVETHAN et al. 2007b).

A turbulent event is basically defined as a series of turbulent fluctuations that contain more energy than the average turbulent fluctuations within a data section. The method detects bursting events within a data section by comparing the absolute value of an instantaneous turbulent flux q (e.g. $q = v_x v_z$) with the standard deviation q' of that flux over the data section. A turbulent event occurs if :

$$|q| > k\, q' \tag{2}$$

where k is a positive constant setting the threshold and q' is the standard deviation of the flux q over the data sample section. NARASIMHA et al. (2007) conducted a sensitivity analysis on the positive multiplier threshold (k). They obtained k =1 to provide good results

in atmospheric boundary layer studies and a similar result was obtained in an estuarine system (TREVETHAN et al. 2007b). Herein k = 1 and consecutive data sections of 10,000 data sample points (200 s at 50 Hz) were used.

For each data section, the information of each detected event encompassed the event start/finish times, duration τ, dimensionless flux amplitude A and relative magnitude m. The event properties were used to compare individual turbulent events within a data set and between synchronised data sets collected simultaneously. Figure 6A introduces the definition of the duration and amplitude of an isolated event. The duration τ of the event is the time interval between the "zeroes" in momentum flux (e.g. $q = v_x v_z$) nearest to the sequence of data points satisfying Equation (2) (Fig. 6A). Practically, the event duration is calculated from the first data point with the same sign as the event to the first data point after the change in sign in momentum flux. The method provides an accurate estimate of the event duration within the limitations of the sampling frequency. The dimensionless amplitude A of an event is the ratio of the averaged flux amplitude during the event to the long-term mean flux of the entire data section :

$$A = \frac{1}{\overline{q}} \int_{t=0}^{\tau} \frac{q}{\tau} dt \tag{3}$$

where $\overline{q}$ is the averaged value of q over the data section, τ is the event duration and $dt = 1/f_{scan}$ (e.g. f_{scan} = 50 Hz). The relative contribution of an event to the total momentum flux of the data section is called the relative magnitude m defined as:

$$m = \frac{A \tau}{T} \tag{4}$$

where T is the total duration of the data section : i.e., T = 200 s for 10,000 samples collected at 50 Hz. This technique was applied to the momentum fluxes $v_x v_y$ and $v_x v_z$, and to the "pseudo" longitudinal suspended sediment flux $v_x i_b$, where i_b is the instantaneous fluctuation in the ADV backscatter intensity.

The method was extended to investigate turbulent sub-events within a large event. For example, in Figure 6A, the turbulent event is characterised by three distinct peaks in momentum flux and the entire event may be represented as a succession of three consecutive "turbulent sub-events". The second sub-event is highlighted with hatching in Figure 6B. A turbulent sub-event was defined when the instantaneous momentum flux within the main turbulent event was greater than the momentum flux threshold (Eq. (2)) of the data section. In Figure 6B, the definition of duration and amplitude of the sub-event are shown. For each sub-event, its start/finish times, duration, dimensionless flux amplitude and relative magnitude were calculated within a given event. The duration of a sub-event is that time interval during which the momentum flux was equal to or greater than the threshold value. For each sub-event, the dimensionless sub-event amplitude is the ratio of the averaged sub-event amplitude to the sub-event duration to the mean flux over the data section. The sub-event properties were calculated for consecutive data sections containing 10,000 data points (200 s at 50 Hz)

along each data set with the same technique used to analyse turbulence events, including the number of sub-events that occurred in each individual event.

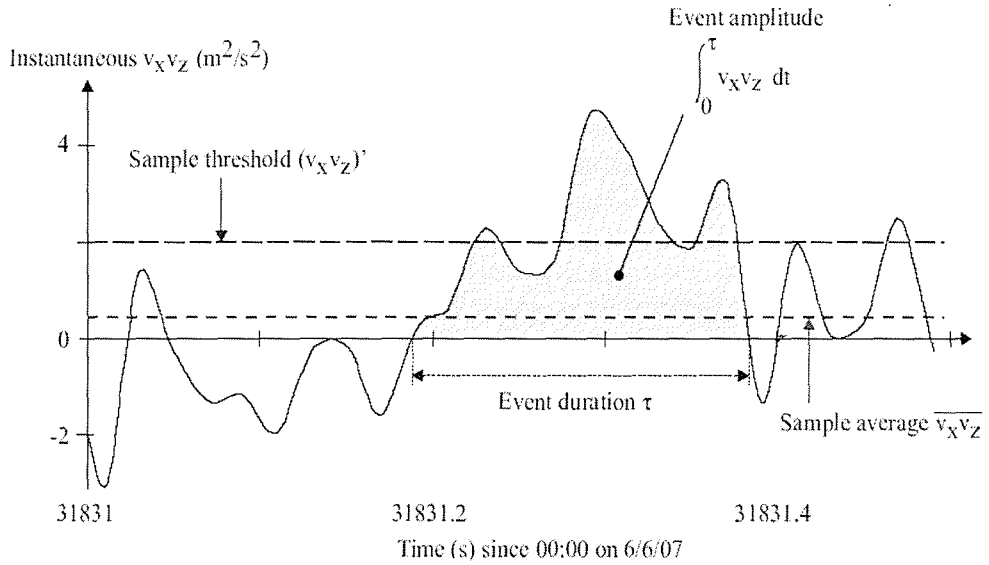

(A) Definition sketch of flux event and event parameters.

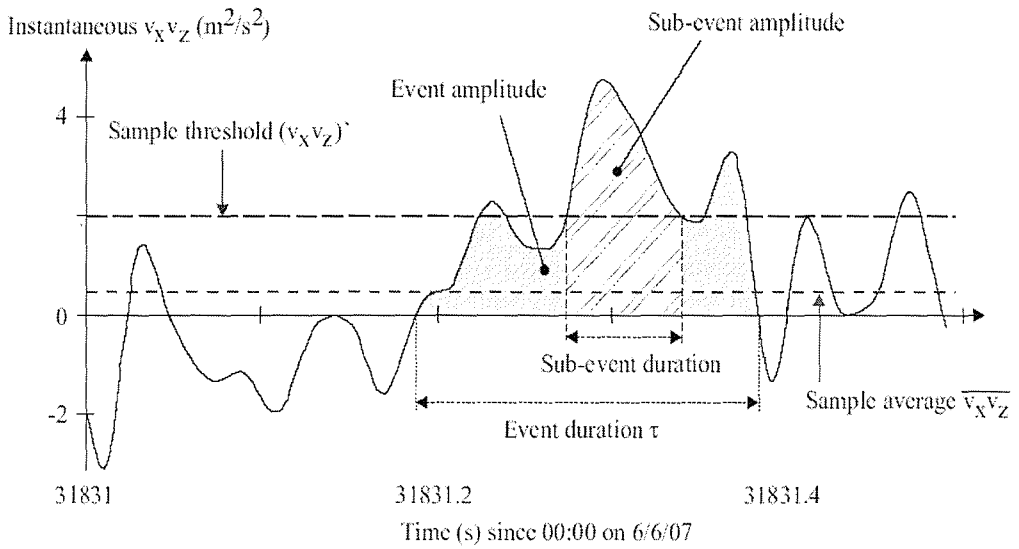

(B) Definition sketch of turbulent sub-events within a turbulent event.

Figure 6. Turbulent flux event definitions and momentum flux data in terms of $v_x v_z$ (study E10, Eprapah Creek, data collected at 0.38 m above bed).

3. TURBULENT FLOW PROPERTIES AT THE MACROSCOPIC SCALES: BASIC PATTERNS

3.1. Basic Flow Properties

The estuarine flow was an unsteady process. The bulk parameters including the water depth and time-average longitudinal velocity were time-dependant and they fluctuate with periods comparable to tidal cycles and other large-scale processes. This is illustrated in Figures 7 and 8 showing the water depth, water conductivity and time-averaged velocities recorded mid-estuary for two field studies in Australia (Eprapah Creek). Figure 7 presents the water depth and conductivity data recorded about mid-estuary during neap tide conditions. The results highlighted some tidal asymmetry during a 24 hours 50 minutes period with a smaller (minor) tidal cycle followed by a larger (major) tidal amplitude. The water conductivity variations were driven primarily by the ebb and flood tides. The moderate range of specific conductivity seen in Figure 7 was typical of a small subtropical estuary under neap tidal conditions in absence of freshwater runoff.

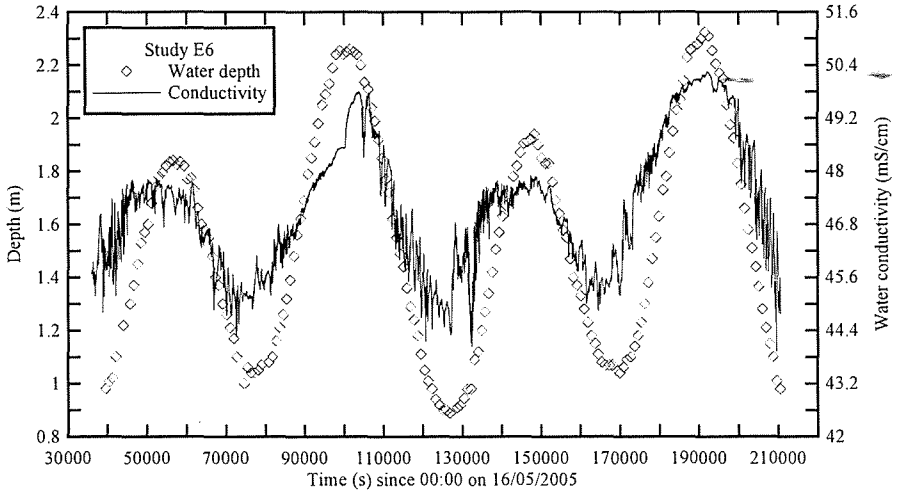

Figure 7. Time variations of the water depth and conductivity in the mid-estuary zone of Eprapah Creek (Australia) during neap tide conditions (study E6).

Figures 8 and 9 present the time-averaged longitudinal velocities in Australia (Fig. 8) and in Japan (Fig. 9). Figure 8 shows data collected in the middle of the deepest channel during spring and neap tides. For all mid-estuary field studies, the largest velocity magnitude occurred just before and after the low tide, with the flood velocities always larger than ebb velocities. KAWANISI and YOKOSI (1994) observed similarly maximum flood and ebb velocities around low tide and larger flood velocities, during some field works in an estuarine channel in Japan. The velocity data showed some multiple flow reversal events around high tides and some long-period oscillations in water elevation and velocity around mid-tide. Figure 8A shows an example of long-period velocity oscillations during the flood tide between t = 105,000 and 125,000 s where the time t is counted since midnight (00:00) on the first day of the study. Figure 8B presents an illustration of multiple flow reversals about high

tide between t = 50,000 and 65,000 s. These low frequency velocity oscillations were possibly generated by some resonance caused by the tidal forcing interacting with the estuary topography and the outer bay system (CHANSON 2003, TREVETHAN 2008). These effects were more noticeable during neap tide conditions and seemed more pronounced in the upper estuary (TREVETHAN et al. 2007a).

At Hamana Lake, the tidal range was small during both spring and neap tidal conditions because the restricted entrance (Fig. 4C) reduced the tidal range observed in the estuary by dampening the ocean tidal oscillations. The difference in tidal range was less than 0.2 m between neap and spring tide studies (Fig. 9). The response of the time-averaged streamwise velocity to the tidal forcing was different between Eprapah Creek and Hamana Lake. Figure 9 shows the time-averaged streamwise velocity and water depth as functions of time in Japan. The maximum flood and ebb velocities at Hamana Lake were observed in the middle of the tide under spring and neap tidal forcing. HAM et al. (2001) observed a similar tidal trend in a shallow semi-enclosed bay. During neap tidal conditions, the maximum flood and ebb velocity suggested a neutral tidal bias (Fig. 9B). However, under spring tidal forcing, the maximum ebb velocity at Hamana Lake was larger than the maximum flood velocity (Fig. 9A).

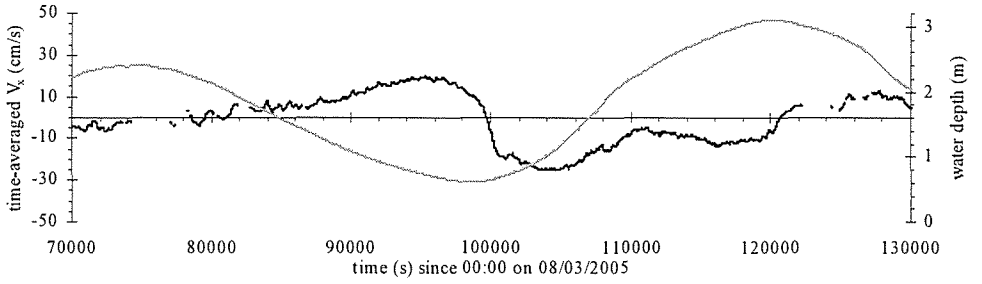

(A) Longitudinal velocity data collected at 0.1 m above the bed during spring tides (study E5).

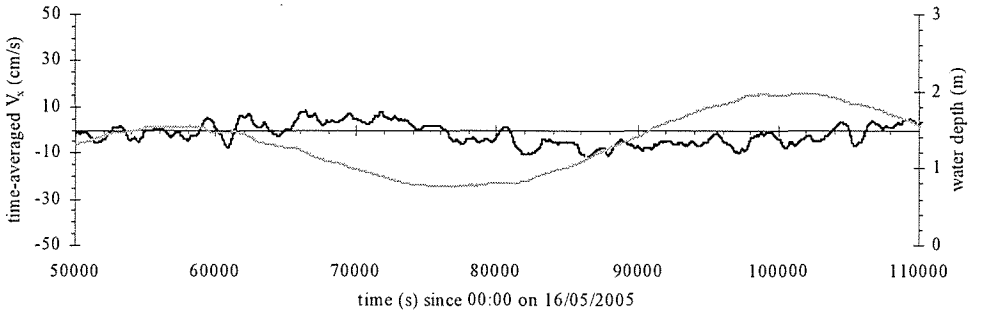

(B) Longitudinal velocity data collected at 0.4 m above the bed during neap tides (study E6).

Figure 8. Time variations of the time-averaged longitudinal velocity $\overline{V_X}$ (positive downstream) and water depth for a full tidal cycle at Eprapah Creek (Australia), mid-estuary zone (site 2B) - Legend: [—] time-averaged longitudinal velocity (cm/s); [—] water depth.

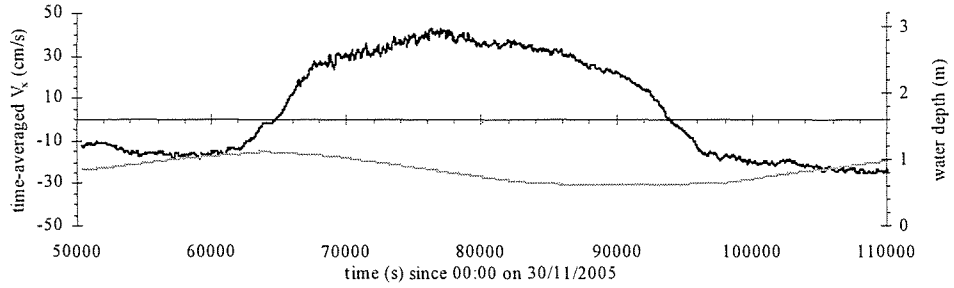

(A) Longitudinal velocity data collected at 0.25 m above the bed during spring tides (study J2).

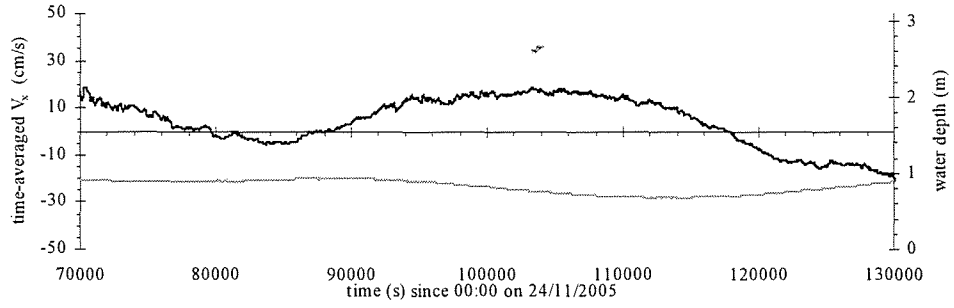

(B) Longitudinal velocity data collected at 0.25 m above the bed during neap tides (study J1).

Figure 9. Time variations of the time-averaged longitudinal velocity $\overline{V_X}$ (positive downstream) and water depth for a full tidal cycle at Hamana Lake (Japan) - Legend: [—] time-averaged longitudinal velocity (cm/s); [---] water depth.

3.2. Turbulence Properties

The field observations showed systematically large standard deviations of all velocity components at the beginning of the flood tide for all tidal cycles. Typical field measurements of standard deviations for the longitudinal velocity v_x' are shown in Figure 10 for two tidal cycles in spring and neap tides in Australia and Japan. Figure 10 shows the magnitude of v_x' from a low water (LW1) to the next low water (LW2), and the data are presented in a circular plot. In such a circular plot, the radial coordinate is the turbulent property v_x' and the angular coordinate is the time relative to the next low water. From the first low water, the time variations of the data progress anticlockwise until the next low water. The high and low waters are indicated: the low waters are the positive horizontal axis, and the high waters are the dotted lines. The upper half of the graph corresponds roughly to the flood tide while the lower half represents the ebb tide.

In Australia, the standard deviations of all velocity components were two to four times larger in spring tides than during neap tides. Figure 10A highlights the large velocity standard deviations in spring tide conditions. The presentation illustrates that v_x' was systematically larger during the flood tide than during the ebb tide, while there were significant fluctuations

in velocity standard deviations during the entire tidal cycle. KAWANISI and YOKOSI (1994) observed similarly larger measured velocity standard deviations during flood tide in a large tidal channel.

At Hamana Lake, the tidal trends of all velocity standard deviations were about the same for spring and neap tidal conditions, but the median values were twice as large during spring tides (Fig. 10B). The observation tended to indicate that the largest velocity standard deviations occurred about the time of maximum longitudinal velocity as noted in TREVETHAN (2008).

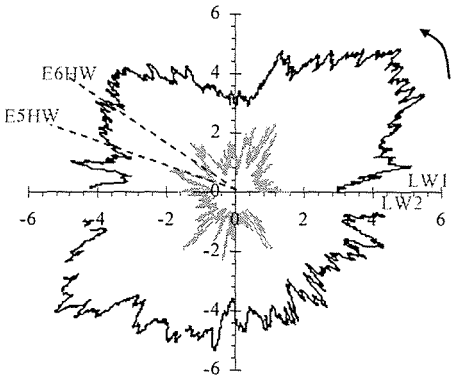

(A) Eprapah Creek (Australia), mid-estuary zone (site 2B), study E5 (0.1 m above bed), and study E6 (0.4 m above bed).

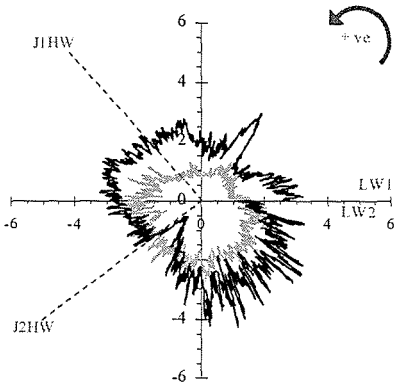

(B) Hamana Lake (Japan).

Figure 10. Time variations of the standard deviations of the longitudinal velocity v_x' (cm/s) during a major tidal cycle in spring and neap tidal conditions: [•] spring tide, and [◦] neap tide - Circular plot from a low water to the next low water - Dotted line: high water.

The horizontal turbulence intensity v_y'/v_x' was approximately equal to 1 for spring and neap tide conditions at both Eprapah Creek and Hamana Lake, indicating that turbulence fluctuations in the longitudinal and transverse directions were of similar magnitude. They were larger than laboratory observations in straight prismatic rectangular channels which yielded $v_y'/v_x' = 0.5$ to 0.7 (NEZU and NAKAGAWA 1993, KOCH and CHANSON 2005),

but the findings were close to recent LES computations in a shallow water channel with similar Reynolds number conditions (HINTERBERGER et al. 2008). The vertical turbulence intensities v_z'/v_x' were similar to the observations of SHIONO and WEST (1987) and KAWANISI and YOKOSI (1994) in estuaries, and of NEZU and NAKAGAWA (1993) and XIE (1998) in laboratory open channels. For all estuarine studies in Australia and Japan, v_z'/v_x' was always smaller than the horizontal turbulence intensity v_y'/v_x' and the result implied some form of turbulence anisotropy.

The skewness and kurtosis gave some information on the temporal distribution of the turbulent velocity fluctuation around its mean value. For all studies, the skewness and kurtosis of all velocity components fluctuated significantly during each tidal cycle. They exhibited some characteristics that differed from the expected skewness and kurtosis for a Gaussian distribution. The normalised third (skewness) and fourth (kurtosis) moments of the velocity fluctuations appeared to be close to the observations of SHIONO and WEST (1987) in an estuary. They were also comparable with the LDV data of NIEDERSCHULTZE (1989) and TACHIE (2001) in developing turbulent boundary layers in laboratory channels.

All tangential Reynolds stresses showed significant fluctuations over the tidal cycles of all field studies undertaken at both estuaries. The turbulent stress $\rho \overline{v_x v_z}$ close to the bed varied with the tides, being predominantly positive during the flood tide and negative during the ebb tide. This trend was consistent with the earlier data of OSONPHASOP (1983), KAWANISI and YOKOSI (1994) and HAM et al. (2001) in tidal channels. The negative correlation between $\rho \overline{v_x v_z}$ and $\overline{V_x}$ was also consistent with traditional boundary layer results (XIE 1998, TACHIE 2001, NEZU 2005). At Eprapah Creek the magnitudes of all tangential Reynolds stresses were at least an order of magnitude larger during spring tides than those observed for neap tidal conditions. The larger magnitude of all Reynolds stresses derived from the increased tidal forcing interacting with the local bathymetry. However, at Hamana Lake, the difference in the magnitude of all Reynolds stresses under spring and neap tidal forcing was not as significant, with Reynolds stress magnitudes being up to twice as large under spring tidal forcing. The smaller difference in spring and neap turbulent stress magnitudes at Hamana Lake was conceivably related to the small difference in tidal amplitude between the field investigations (Table 1).

The standard deviations of all tangential Reynolds stresses increased with increasing longitudinal velocity magnitude. At Eprapah Creek (Australia), the magnitude of all tangential Reynolds stress standard deviations were one order of magnitude greater under spring tidal forcing than those observed during neap tides. At Hamana Lake (Japan), the spring tidal tangential Reynolds stress standard deviations were approximately twice as large as those measured under neap tidal conditions. The results obtained in both estuaries showed that the probability distribution functions of all tangential Reynolds stresses were not Gaussian.

3.3. Turbulence Time Scales

The integral time scale of a velocity component is a measure of the longest connection in the turbulent behaviour of that velocity component. Some variations of longitudinal integral time scales T_{Ex} are shown in Figure 11 for a major tidal cycle during neap and spring tide

conditions. Note that the axes have a logarithmic scale and the units are milliseconds. At Eprapah Creek significant fluctuations in the horizontal integral time scales were observed throughout the tidal cycles, with the integral time scales observed under neap tidal conditions being larger than those for spring tides (Figure 11). The horizontal integral times at Eprapah Creek ranged between 0.06 s and 1.0 s with a median value of approximately 0.15 s under spring tides and between 0.06 s and 2.40 s (median value: 0.31 s) during neap tidal conditions. In Hamana Lake, the fluctuations in horizontal integral time scales over the tidal cycle were relatively small. The horizontal integral time scales ranged between 0.2 s and 1.5 s under both spring and neap tides (Figure 11). The median values of longitudinal and transverse integral time scales at Hamana Lake were approximately 0.75 a and 0.58 s under spring and neap tidal conditions respectively.

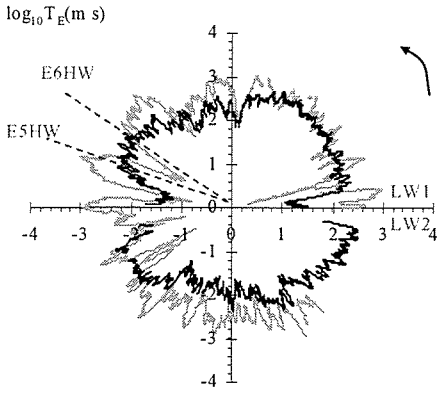

(A) Eprapah Creek (Australia), mid-estuary zone (site 2B), study E5 (0.1 m above bed), and study E6 (0.4 m above bed).

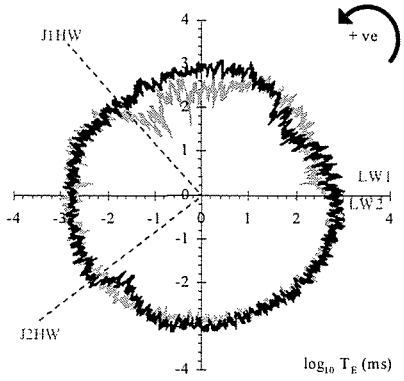

(B) Hamana Lake (Japan), 0.28 m above the bed.

Figure 11. - Time variations of the integral time scale T_{Ex} (units: ms) for V_x during a major tidal cycle for neap and spring tidal conditions - The axes have a logarithmic scale - Legend: [•] spring tide; [◦] neap tide.

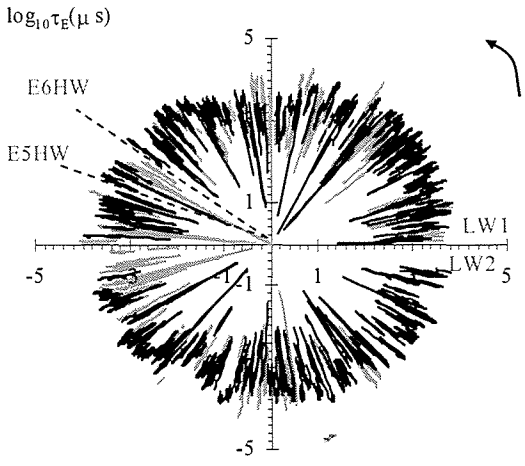

(A) Eprapah Creek (Australia), mid-estuary zone (site 2B), study E5 (0.1 m above bed), and study E6 (0.4 m above bed).

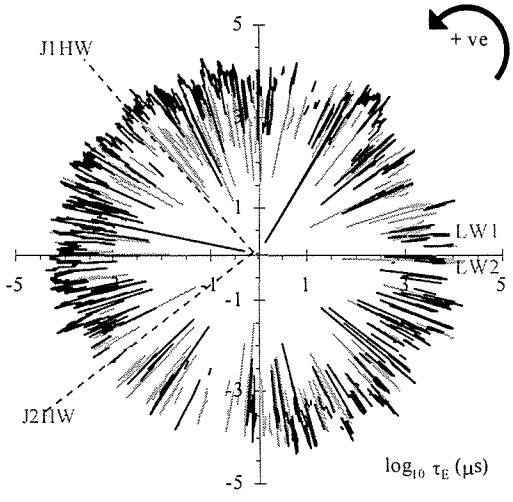

(B) Hamana Lake (Japan), 0.28 m above the bed.

Figure 12. Time variations of the dissipation time scale τ_{Ex} (units μs) for V_x during a major tidal cycle for neap and spring tidal conditions - The axes have a logarithmic scale - Legend: [•] spring tide; [◦] neap tide.

The dissipation time scale, also called Taylor micro scale, is a measure of the most rapid changes that occur in the fluctuations of a velocity component. It is a characteristic time scale of the smaller eddies which are primary responsible for the dissipation of energy. Figure 12 shows the variations of longitudinal dissipation time scales τ_{Ex} for a major tidal cycle during neap and spring tide conditions in Australia and in Japan. The axes have a logarithmic scale

and the units are in microseconds. At both estuaries, the dissipation time scale data seemed independent of the tidal phase with horizontal dissipation time scales between 0.0001 s and 0.03 s for all field studies (Fig. 12). The dissipation time scales at Eprapah Creek seemed independent of the tidal conditions, vertical and longitudinal sampling locations, with median values typically between 0.002 s and 0.003 s. At Hamana Lake, the median values of the horizontal dissipation time scales (τ_{Ex} and τ_{Ey}) were between 0.007 s and 0.011 s for spring tidal conditions, and between 0.004 s and 0.006 s during neap tidal conditions. The horizontal dissipation time scales were slightly different, and the median values of transverse dissipation time scales τ_{Ey} were larger than the median values of longitudinal dissipation time scales τ_{Ex} under spring and neap tidal forcing. Note that the dissipation time scales were consistently smaller than the time between two consecutive samples: e.g., $1/f_{scan}$ = 0.04 s for f_{scan} = 25 Hz in Figure 12. The findings highlighted that a high frequency sampling is required and the sampling rates must be at least 20 to 30 Hz to capture a range of eddy time scales relevant to the dissipation processes.

The analysis of the integral and dissipation time scales of all velocity components showed no obvious trend with tidal phase under both neap and spring tidal forcing. During the present field studies at Hamana Lake and Eprapah Creek, the dimensionless transverse and vertical dissipation time scales were respectively: $T_{Ey}/T_{Ex} \sim 1$ and $T_{Ez}/T_{Ex} \sim 1$ to 3. In a tidal channel in Southern Australia, OSONPHASOP (1983) observed $T_{Ey}/T_{Ex} \sim 1.7$ and $T_{Ez}/T_{Ex} \sim 2.2$.

3.4. Dimensionless Turbulence Parameters

For most turbulence properties, the spring tidal data at Eprapah Creek were larger and showed a more asymmetrical tidal response. For example, the standard deviations of longitudinal velocity under spring tidal conditions were larger at Eprapah Creek than at Hamana Lake, despite the larger longitudinal velocity observed at Hamana Lake (Fig. 8, 9 and 10). The ratio of local tidal amplitude and local mean depth at the experimental site a_1/h_1 may assist with the understanding of this phenomenon (TREVETHAN 2008).

Dimensionless turbulence parameters are commonly used in turbulence investigations to compare the relative turbulence characteristics of different systems under distinct flow conditions. Table 2 regroups the median values of basic dimensionless turbulence properties in Australia and Japan. The dimensionless turbulence parameters include the turbulent intensity ratios (v_y'/v_x', v_z'/v_x'), the relative turbulence intensities of the longitudinal, transverse and vertical velocity fluctuations ($v_x'/|\overline{V_x}|$, $v_y'/|\overline{V_x}|$, $v_z'/|\overline{V_x}|$), the normalized tangential Reynolds stresses ($|\overline{v_x v_z}|/\overline{V_x}^2$, $|\overline{v_x v_y}|/\overline{V_x}^2$, $|\overline{v_y v_z}|/\overline{V_x}^2$), the magnitude of correlation coefficients of Reynolds stresses ($|R_{vxvz}|$, $|R_{vxvy}|$, $|R_{vyvz}|$) and the dimensionless integral time scales ($T_{Ex}\sqrt{g/h_1}$, $T_{Ey}\sqrt{g/h_1}$, $T_{Ez}\sqrt{g/h_1}$).

Table 2. Median values of dimensionless turbulence parameters over the full investigation periods for the field studies undertaken in Australia (Eprapah Creek) and Japan (Hamana Lake).

Estuary	Eprapah Creek		Hamana Lake	
Field Study	E5	E6	J1	J2
Tidal Conditions	Spring	Neap	Neap	Spring
Tidal range (m)	2.37	1.36	0.39	0.56
a_1/h_1	0.76	0.43	0.22	0.31
v_y'/v_x'	1.00	0.89	0.83	0.86
v_z'/v_x'	0.39	0.51	0.52	0.56
$v_x'/\lvert\overline{V_x}\rvert$	0.42	0.21	0.15	0.13
$v_y'/\lvert\overline{V_x}\rvert$	0.44	0.19	0.15	0.13
$v_x'/\lvert\overline{V_x}\rvert$	0.16	0.11	0.07	0.07
$\lvert\overline{v_x v_z}\rvert/\overline{V_x}^2$	0.014	0.005	0.004	0.004
$\lvert\overline{v_x v_y}\rvert/\overline{V_x}^2$	0.014	0.004	0.003	0.002
$\lvert\overline{v_y v_z}\rvert/\overline{V_x}^2$	0.004	0.002	0.001	0.001
$\lvert R_{vxvy}\rvert$	0.08	0.13	0.20	0.27
$\lvert R_{vxvz}\rvert$	0.23	0.17	0.31	0.30
$\lvert R_{vyvz}\rvert$	0.07	0.10	0.13	0.20
$T_{Ex}\sqrt{g/h_1}$	0.43	0.59	2.45	2.50
$T_{Ey}\sqrt{g/h_1}$	0.30	0.93	1.86	1.94
$T_{Ez}\sqrt{g/h_1}$	0.72	2.06	1.98	1.39

The dimensionless turbulence data suggested a different set of turbulence and mixing properties when $a_1/h_1 > 0.5$ (Table 2), while the magnitudes of relative turbulence intensities and normalised Reynolds stresses were similar for $a_1/h_1 < 0.5$. Previous turbulence studies in

large estuarine systems (e.g. BOWDEN and HOWE 1963, OSONPHASOP 1983, WEST and ODUYEMI 1989) yielded results of $v_x'/|\overline{V_x}| < 0.15$ and $|\overline{v_x v_z}|/\overline{V_x}^2 < 0.004$, that were similar to those observed at Hamana Lake and Eprapah Creek when $a_1/h_1 < 0.5$. The findings indicated that the turbulence properties of estuaries with $a_1/h_1 < 0.5$ could not be applied to shallow-water estuaries where $a_1/h_1 > 0.5$.

3.5. Suspended Sediment Fluxes

For some field studies in Australia (Eprapah Creek), an acoustic Doppler velocimeter (ADV) was calibrated in terms of the backscatter intensity versus suspended sediment concentration (SSC) (CHANSON et al. 2008a). The results enabled a characterisation of the fluctuations in suspended sediment concentrations for two field studies (E6 and E7).

The instantaneous suspended sediment concentration (SSC) showed some large fluctuations throughout the entire field studies, including during the tidal slacks (high and low tides). The data tended to indicate larger suspended loads during the early flood tides. The data showed also some low frequency oscillation patterns in terms of the SSC that may be linked with the low frequency fluctuations of the streamwise velocity. In the middle and upper estuarine zones, the ratio $SSC'/\overline{SSC}$ was respectively 0.66 and 0.57 on average, where $\overline{SSC}$ is the time-averaged suspended sediment concentration and SSC' is its standard deviation.

The instantaneous advective suspended sediment flux per unit area q_s was calculated as :

$$q_s = SSC\ V_x \tag{5}$$

where q_s and V_x are positive in the downstream direction, and the suspended sediment concentration SSC is in kg/m^3. q_s is a local measure of the suspended sediment flux at the ADV sampling site. Typical instantaneous suspended sediment flux per unit area results are presented in Figure 13. The data characterise the advective suspended sediment flux per unit area in a sampling volume located at 0.2 m above the bed.

The sediment flux per unit area data showed typically an upstream, negative suspended sediment flux during the flood tide and a downstream, positive suspended sediment flux during the ebb tide. The instantaneous suspended sediment flux per unit area data q_s showed considerable time-fluctuations that derived from a combination of velocity and suspended sediment concentration fluctuations. The data demonstrated further some high frequency fluctuation with some form of suspended sediment flux bursts that were likely linked to and caused by some turbulent bursting phenomena next to the bed. Some low frequency fluctuations in suspended sediment flux were also observed. In the middle estuary, the magnitude of suspended sediment fluxes were about one order of magnitude larger than those observed in the upper estuary.

For each tidal period of 24 hour 50 min., the suspended sediment flux per unit area data were integrated with respect of time. The results gave the net sediment mass transfer per unit area at the sampling volume:

$$m_s = \int_{24h50min} q_s \, dt \tag{6}$$

For both field studies E6 and E7, the net sediment mass transfer per area was negative (i.e. upstream). In the middle estuary, Equation (6) yielded m_s = -22.3 and -20.8 kg/m^2 for each 24 h 50 min tidal period, while Equation (6) gave m_s = -6.66 and -1.81 kg/m^2 in the upper estuary. That is, the net sediment flux over a full tidal cycle corresponded on average to an upstream net suspended sediment transfer. Several researchers investigated the net suspended sediment flux in estuaries of subtropical and tropical river estuaries during similar dry conditions and tidal ranges. Previous results showed a similar net upstream sediment transfer in dry weather: e.g., LARCOMBES and RIDD (1992), HOSSAIN et al. (2001), KAWANISI et al. (2006). However, during rain storms and wet weather the net sediment mass flux is positive in the downstream direction in such estuarine systems.

A striking feature of the analysed data sets is the large fluctuations in the suspended sediment fluxes during the tidal cycles. This feature was rarely documented, but an important feature of the data sets is that the present data were collected continuously at high frequency (25 and 50 Hz) during relatively long periods. It is however acknowledged that the data were point measurements. Any extrapolation would imply that the sampling volume was representative of the entire channel cross-section.

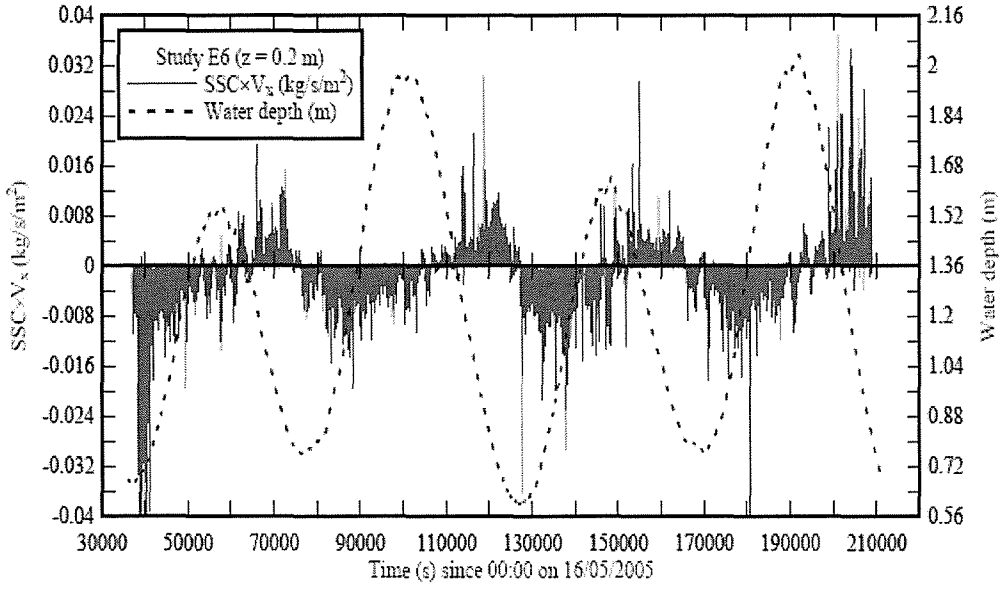

Figure 13. Time variations of the instantaneous suspended sediment flux per unit surface area (SSC×V_x, positive downstream) and measured water depth during the study E6 (neap tide) at 0.2 m above bed.

The integral time scale of the suspended sediment concentration (SSC) data represents a characteristic time of turbid suspensions in the creek. Calculations were performed for two field studies in Australia (E6 and E7). The SSC integral time scale data seemed relatively independent of the tidal phase and yielded median SSC integral time scales T_{ESSC} of about 0.06 s.

A comparison between the turbulent and SSC integral time scales showed some difference especially during the ebb tide. In the mid-estuarine zone, the ratio of SSC to turbulent integral time scales was on average T_{Essc}/T_{Ex} = 0.21 and 0.14 during the flood and ebb tides respectively. In the upper estuary, the ratio T_{Essc}/T_{Ex} was about T_{Essc}/T_{Ex} = 1 and 0.18 during the flood and ebb tides respectively. Basically the ratio T_{Essc}/T_{Ex} was about 2 to 5 times lower during ebb tide periods. The findings tended to suggest that the sediment suspension and suspended sediment fluxes were dominated by the turbulent processes during the flood tide, but not during the ebb tide. The experimental results showed further some fluctuations in SSC integral time scales during the tidal cycle.

These data sets provided simultaneous turbulence and suspended sediment concentration measurements recorded continuously at high frequency for 50 hours per investigation. The data analyses yielded an unique characterisation of the turbulent mixing processes and suspended sediment fluxes. The integral time scales for turbulence and suspended sediment concentration were about equal during flood tides, but differed significantly during ebb tides. The same pattern might take place with other scalars and be pertinent to the turbulent mixing modelling in shallow-water subtropical estuaries under dry-weather conditions.

3.6. Discussion

The boundary shear stress may be estimated from the velocity gradient next to the bed, although other techniques may be used (SCHLICHTING 1979, MONTES 1998, KOCH and CHANSON 2005). The near-bed velocity shear stress is calculated as:

$$\tau_o = \rho \left(\frac{\kappa (V_x)_1}{Ln \frac{z_1}{k_s}} \right)^2 \quad (7)$$

where ρ is the fluid density, $(V_x)_1$ is the time-averaged longitudinal velocity of the ADV unit located closest to the bed (z_1 = 0.13 m, study E10), κ is the von Karman constant (κ = 0.4) and k_s is the equivalent roughness height. At Eprapah Creek (Australia), the river bed in the middle estuarine zone consisted of gravels and sharp rocks corresponding to $k_s \approx 10$ mm. Experimental results indicated that the boundary shear stress was maximum during the early flood tide and end of ebb tide when the measured longitudinal velocity amplitude was the largest. For the entire field study E10, the median shear stress was τ_o = 0.0052 Pa. For the same study, the boundary shear stress data may be compared with the tangential Reynolds stress $\rho \overline{v_x v_z}$ measured simultaneously at z_2 = 0.38 m, as well as with the velocity gradient shear stress measured between z_1 = 0.13 m and z_2 = 0.38 m :

$$\tau_{12} = \rho \left(\frac{\kappa((V_x)_2 - (V_x)_1)}{\mathrm{Ln}\frac{z_2}{z_1}} \right)^2 \quad (8)$$

For the entire study E10, the tangential Reynolds stress and the median velocity gradient shear stress (Eq. (8)) were respectively: $\rho \overline{v_x v_z}$ = 0.02 Pa and τ_{12} = 0.052 Pa. For comparison, the median tangential shear stresses $\rho \overline{v_x v_y}$ measured at z = 0.13 m and 0.38 m were 0.024 Pa and 0.031 Pa respectively.

The findings implied that the turbulent shear between 0.13 m ≤ z ≤ 0.38 m was one order of magnitude larger than the boundary shear stress (Eq. (7)). The observation differed from turbulence data collected in a laboratory channel, but a key feature of natural estuary flows was the significant three-dimensional effects associated with strong secondary currents.

During several field studies, some anomalies were observed in terms of the transverse velocity data. For example, during the study E10, the time-averaged transverse velocities $\overline{V_y}$ recorded at z = 0.13 m and 0.38 m flowed at times in opposite directions for relatively long durations (e.g. Fig. 14). These anomalies were observed during the flood and ebb tides, and around low tides for the entire study.

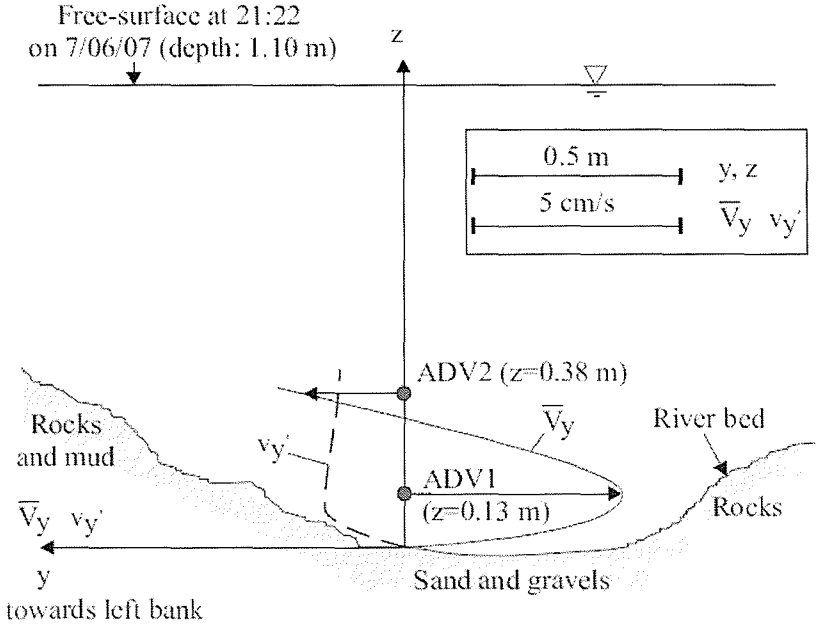

Figure 14. Transverse shear flow pattern in the mid-estuarine zone of Eprapah Creek: dimensioned sketch of the vertical profiles of transverse velocity $\overline{V_y}$ and turbulent velocity v_y' at the sampling site during the early flood tide in Australia (study E10).

These observations highlighted the occurrence of some secondary currents associated with strong transverse shear and large tangential stresses $\rho \overline{v_x v_y}$ at the sampling location. An example of transverse velocity anomaly is presented in Figure 14. The flow pattern sketched in Figure 14 shows the vertical profiles of transverse velocity $\overline{V_y}$ and of turbulent velocity v_y' next to the channel bed, where v_y' is the standard deviation of the transverse velocity. The transverse shear pattern sketched in Figure 14 was associated with large normal and tangential stresses $\rho \overline{v_y v_y}$ and $\rho \overline{v_x v_y}$ at both z = 0.13 m and 0.38 m for that study.

TREVETHAN (2008) discussed the formation the transverse velocity anomalies in Eprapah Creek, their collapse and reformation in the opposite direction. He suggested that the alternance in transverse shear anomalies was linked with the long-period oscillations induced by seiching resonance in the outer bay system (Moreton Bay).

4. TURBULENT FLOW PROPERTIES AT THE MICROSCOPIC SCALES: TURBULENT EVENTS

4.1. Presentation

While the turbulence is often characterised by its statistical moments, it is not a Gaussian process. Turbulent flows are dominated by coherent structure activities and turbulent events. A turbulent event may be defined as a series of turbulent fluctuations containing more energy than the average turbulent fluctuations. The turbulent events are often associated with coherent flow structures such as eddies and bursting (KLINE et al. 1967, RAO et al. 1971). These events play a major role in terms of sediment scour, transport and accretion as well as contaminant mixing and dispersion (NIELSEN 1992, NEZU and NAKAGAWA 1993, CHANSON 2004). Turbulent event analyses were successfully applied to laboratory open channel flows (NEZU and NAKAGAWA 1993), wind tunnel studies (OSTERLUND et al. 2003) and atmospheric boundary layer flows (FINNIGAN 2000, NARASIMHA et al. 2007). They were however rarely applied to unsteady open channel flows and estuaries.

For a field study (study E10, Eprapah Creek), a detailed turbulent event analysis was conducted (section 2.6). Figure 15 illustrates a time series of the dimensionless flux amplitude of $v_x v_z$ from a data set as a function of time for a 10 s sample during the early flood tide. The data presentation shows the duration and dimensionless amplitude of each event in a simplified format. It is seen that the time series includes both positive and negative turbulent events, each event corresponding to a rectangular pulse. The pulse width is the duration τ and the height is the dimensionless amplitude A, while the area beneath is proportional to the event magnitude m.

The turbulent events and sub-events were investigated specifically for the turbulent fluxes $v_x v_z$, $v_x v_y$, and $v_x i_b$, for the study E10 conducted mid-estuary in Eprapah Creek (Australia). Table 3 summarises the number of events and sub-events detected by the ADV units for the entire study (50 hours). For the whole data set, the histograms of event duration, event amplitude, sub-event duration and sub-event amplitude were calculated. Figure 16

shows the normalised probability distribution functions of event duration τ and dimensionless event amplitude A for the momentum fluxes $v_x i_b$.

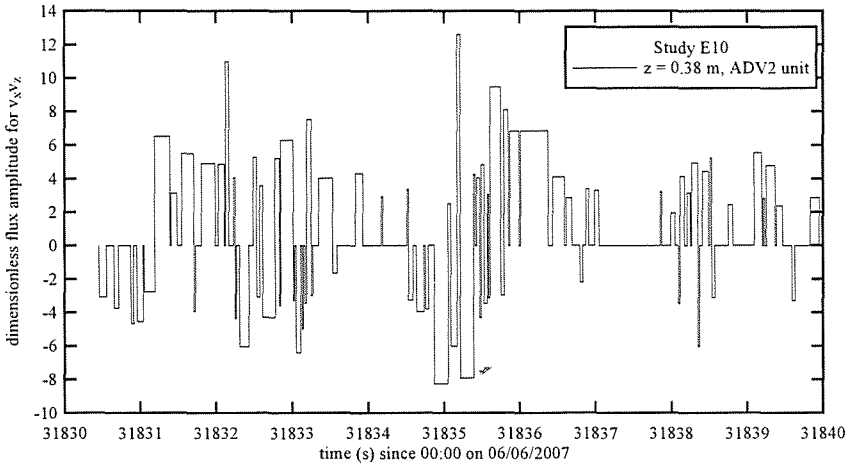

Figure 15. Dimensionless amplitude of detected turbulent events in terms of $V_x V_z$ (Study E10, 0.38 m above the bed).

During the field study, the majority of turbulent events had a duration between $0.08 < \tau < 0.3$ s for all momentum fluxes. On average, the turbulent event duration was about 0.2 s. The distributions of event amplitude presented a similar shape for the fluxes $v_x v_z$ and $v_x v_y$. For the entire study and all fluxes, the median amplitude magnitude was between $3 \leq |A| \leq 14$. For each turbulent flux, the event amplitude distribution tended to indicate a larger proportion of positive events than of negative events for all ADV units. Next to a boundary, the turbulent bursting process is composed of a quasi-periodic cycle of ejections and sweep motions (NEZU and NAKAGAWA 1993, PIQUET 1999). Ejections and sweeps corresponded to a negative amplitude in Figure 16B, while a positive event amplitude implied a wallward or outward interaction. The data sets for the field study E10 suggested comparatively a larger number of interaction events than sweep and ejection events. However, for all the fluxes, the positive events ($A > 0$) were on average longer and of smaller amplitude than the negative events ($A < 0$), with a similar event magnitude overall (Table 4). Table 4 summarises the median values of number of events per sample, event duration, dimensionless event amplitude, and relative event magnitude for each ADV unit. (The exact location of each sampling volume is given in Table 3, column 1.) Although there were some differences between the three velocimeters (Table 4), the statistical results were relatively close and tended to show little effect of the sampling volume location.

4.2. Turbulence Event and Sub-Event Statistics

The turbulent event statistics were collected over a 200 s sample (10,000 data points) every 10 s along the entire ADV data sets. The event statistics including the number of events per sample, median event duration, amplitude and relative magnitude were sampled in a

similar fashion to all turbulence properties, thereby allowing for observations of any tidal trend.

For the entire study, there were on average 1 to 4 turbulent events per second for all the fluxes (Table 4). This result was close for all ADV units and somehow consistent with the early results of RAO et al. (1971). For all momentum fluxes and all ADV units, the number of events per sample varied in a similar pattern with the tides. The number of events per sample increased about low tide when the water column was shallower and the effects of bed shear stress were stronger, while it decreased about high tide.

Table 3. Total number of turbulent events and sub-events detected in the ADV data sets for the entire study E10 (Eprapah Creek, Australia).

ADV unit (1)	Flux (2)	Number of events (3)	Number of sub-events (4)
ADV1 (z=0.13 m, 10.70 m from left bank)	$v_x v_y$	164,706	479,376
	$v_x i_b$	640,046	741,963
ADV2 (z=0.38 m, 10.70 m from left bank)	$v_x v_z$	389,113	712,283
	$v_x v_y$	762,090	982,352
	$v_x i_b$	889,305	743,320
ADV3 (z=0.38 m, 10.78 m from left bank)	$v_x v_z$	542,861	829,317
	$v_x v_y$	242,939	588,094
	$v_x i_b$	885,940	902,951

Table 4. Turbulent event characteristics for all ADV units during the entire study E10.

Parameter	ADV1 unit		ADV2 unit			ADV3 unit		
	$v_x v_y$	$v_x i_b$	$v_x v_z$	$v_x v_y$	$v_x i_b$	$v_x v_z$	$v_x v_y$	$v_x i_b$
(1)	(2)	(3)	(4)	(5)	(6)	(7)	(8)	(9)
Nb of events per data sample	154	743	389	912	988	614	221	1,050
Event duration τ (s)								
Median duration of positive events (A > 0) (s)	0.26	0.10	0.12	0.10	0.08	0.10	0.16	0.40
Median duration of negative events (A < 0) (s)	0.18	0.10	0.10	0.08	0.06	0.08	0.12	0.08
Event amplitude A								
Median amplitude of positive events (A > 0)	3.34	11.87	3.44	3.87	11.9	3.56	3.26	11.04
Median amplitude of negative events (A < 0)	-4.21	-13.34	-4.06	-4.67	-13.3	-4.31	-4.08	-12.19
Relative magnitude m								
Median magnitude of positive events (A > 0)	0.0048	0.0069	0.0026	0.0021	0.0055	0.0023	0.0033	0.0055
Median magnitude of negative events (A < 0)	-0.0045	-0.0067	-0.0023	-0.0020	-0.0052	-0.0023	-0.0030	-0.0053

Note: data sample length = 200 s (10,000 data points).

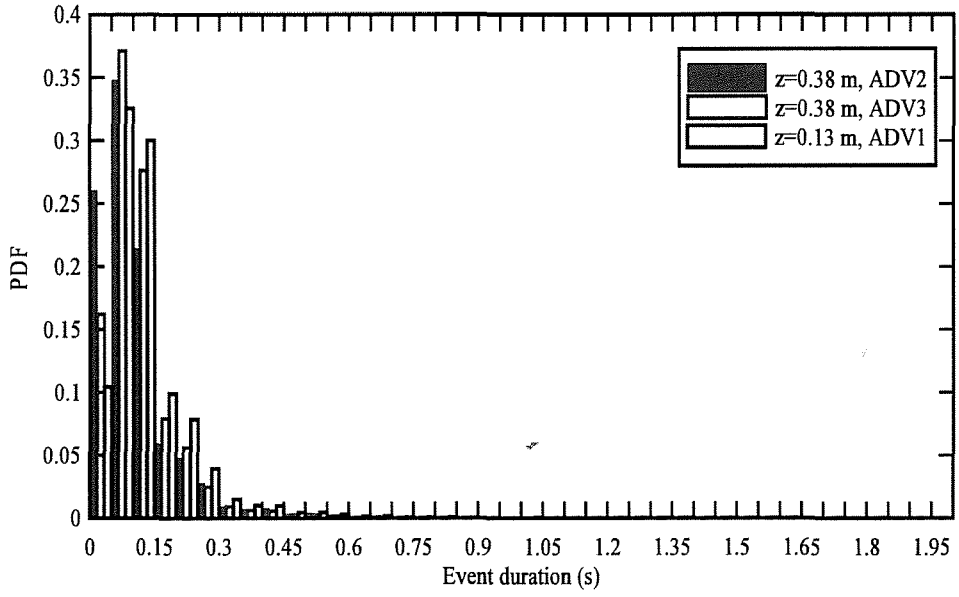

(A) Event duration with histogram intervals of 0.05 s.

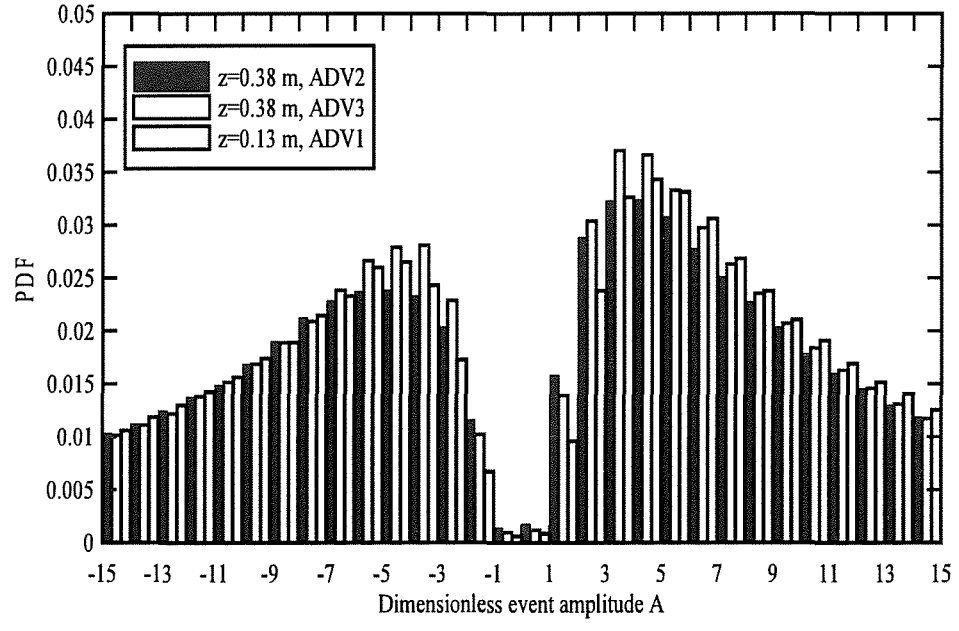

(B) Dimensionless event amplitude with histogram intervals of 1.

Figure 16. Normalised probability distribution functions of event duration and dimensionless amplitude for the suspended sediment flux $v_x i_b$ - Data collected by all ADV units (study E10).

The event duration for the momentum fluxes $v_x v_z$ and $v_x v_y$ seemed to vary with the tides for all the ADV systems, while the pseudo suspended sediment flux data $v_x i_b$ showed no discernable tidal pattern. The magnitude of dimensionless event amplitude for the momentum flux $v_x v_z$ tended to be larger about low water and smaller about high water. No discernable tidal patterns in terms of event amplitude of $v_x v_y$ and $v_x i_b$ fluxes were observed for all ADV units.

For the turbulent sub-events, the median values of the number of sub-events per sample, the sub-event duration, dimensionless sub-event amplitude, and the relative sub-event magnitude are summarized in Table 5. The median sub-event duration was 0.04 s for all fluxes and ADV units, implying that most sub-events had a short life span. The dimensionless sub-event amplitudes for the fluxes $v_x v_z$ and $v_x v_y$ were typically between 2.8 and 6.4, but the sub-event amplitudes for the suspended sediment flux $v_x i_b$ were larger, between 11 and 16 (Table 5).

Table 5. Median sub-event characteristics for all ADV units during the entire study E10.

Parameter	ADV1 unit		ADV2 unit			ADV3 unit		
	$v_x v_y$	$v_x i_b$	$v_x v_z$	$v_x v_y$	$v_x i_b$	$v_x v_z$	$v_x v_y$	$v_x i_b$
(1)	(2)	(3)	(4)	(5)	(6)	(7)	(8)	(9)
Nb of sub-events per data sample	540	982	910	1,375	1,195	1,107	707	1,284
Sub-event duration (s)								
Median duration of positive sub-events (A > 0) (s)	0.04	0.04	0.04	0.04	0.04	0.04	0.04	0.04
Median duration of negative sub-events (A < 0) (s)	0.04	0.04	0.04	0.04	0.04	0.04	0.04	0.04
Sub-event amplitude A								
Median amplitude of positive sub-events (A > 0)	2.83	12.67	3.18	4.09	11.81	3.57	2.76	11.55
Median amplitude of negative sub-events (A < 0)	-5.28	-15.98	-4.84	-6.37	-15.38	-5.41	-5.08	-14.65
Sub-event magnitude m								
Median magnitude of positive sub-events (A > 0)	0.0009	0.0033	0.0009	0.0010	0.0029	0.0010	0.0008	0.0029
Median magnitude of negative sub-events (A < 0)	-0.0014	-0.0038	-0.0012	-0.0015	-0.0035	-0.0013	-0.0013	-0.0034

For all fluxes and all ADV units, the number of sub-events per sample varied in a similar fashion with the tides. That is, the number of sub-events increased about low tide and decreased about high tide. Altogether the variation of the number of sub-events per sample exhibited a similar tidal pattern to that of the number of events per sample. For the entire field study (50 hours), the events durations showed no obvious tidal trend while, for the sub-event amplitude, only those of the momentum flux $v_x v_z$ seemed to vary with the tide. The sub-event

amplitude of the flux $v_x v_z$ showed a similar tidal trend to that of the event amplitude for $v_x v_z$, being largest about low tide and smallest about high tide. On average over the entire study, the results showed 1 to 3 sub-events per turbulent event and the finding was independent of the tidal period.

4.3. Discussion

The turbulent event results in the small estuary of Eprapah Creek may be compared with the field data of RUDRA KUMAR et al. (1995) in an atmospheric boundary layer, re-analysed by NARASIMHA et al. (2007). That study was based upon data collected at Jodhpur with an acoustic anemometer located 4 m above the ground. The comparative results are discussed herein in terms of the momentum flux events for $v_x v_z$ and the basic results are summarised in Table 6.

Table 6. Momentum flux event analyses in terms of $v_x v_z$: comparative results.

Parameters	Eprapah Creek (study E10) TREVETHAN et al. (2007b)	Jodhpur, India NARASIMHA et al. (2007)
(1)	(2)	(3)
z (m)	0.38	4
Mean momentum flux (m^2/s^2)	$2.1\ 10^{-5}$	0.191
Ratio r.m.s/mean	2.98	3.04
Sweep ejection period	40%	36%
Wallward/inward interaction period	16.6%	15%
Idle/passive period	43.4%	49%
Average duration of positive events (A > 0) (s)	0.12	1.71
Average duration of negative events (A < 0) (s)	0.10	1.12
Outer time scale (s)	~ 15 (mode)	~ 30

The experimental data showed that the duration of the events was of the order of 0.11 s and 1.4 s respectively for the estuary and atmospheric studies, compared to an outer time scale of the order of 15 s and 30 s respectively. In the small estuary, the outer time scale was based upon the measured water depth and the velocity magnitude recorded at z = 0.38 m. Hence the outer time scale estimate was a very rough average and could vary over a wide range from as low as 3 s to over 100 s. Overall the differences between turbulent event durations and outer time scales were comparable for both environmental flow studies.

The probability distribution functions of event duration tended to follow a log-normal distribution for both studies. But the probability distribution functions of event magnitude presented some marked difference between estuarine flow data and atmospheric flow results,

with a much narrower event magnitude distribution, as well as a different PDF shape, in the estuarine system.

The relationship between turbulent event amplitude and duration illustrated little correlation between the event amplitude and the event duration. That is, there were a wide range of event amplitudes for any given event duration, and conversely. The observation was valid for both studies and implied that the size of an event, represented by its dimensionless amplitude, and its duration may be considered as two independent parameters.

In the estuarine turbulent flow, the probability distribution functions of the number of turbulent sub-events per burst event were skewed with a very large proportion of events having between 1 and 2 sub-events for all fluxes. The probability distribution functions had however a long tail of small numbers of turbulent events with large numbers of sub-events. This is illustrated in Figure 17 presenting the normalised PDF for the number of sub-events per events for all fluxes at z = 0.38 m. For the momentum flux $v_x \times v_z$, the average number of sub-events per event was 1.21 for that data set, and the maximum number of sub-events per event was 440, with 5,420 turbulent events having 40 sub-events or more for the entire study. Overall the distribution of "extreme" numbers of sub-events per turbulent event showed no tidal trend or correlation with the longitudinal velocity V_x.

The data analyses demonstrated the significance of turbulent events in environmental flows and showed the complex nature of bursting events consisting of consecutive sub-events.

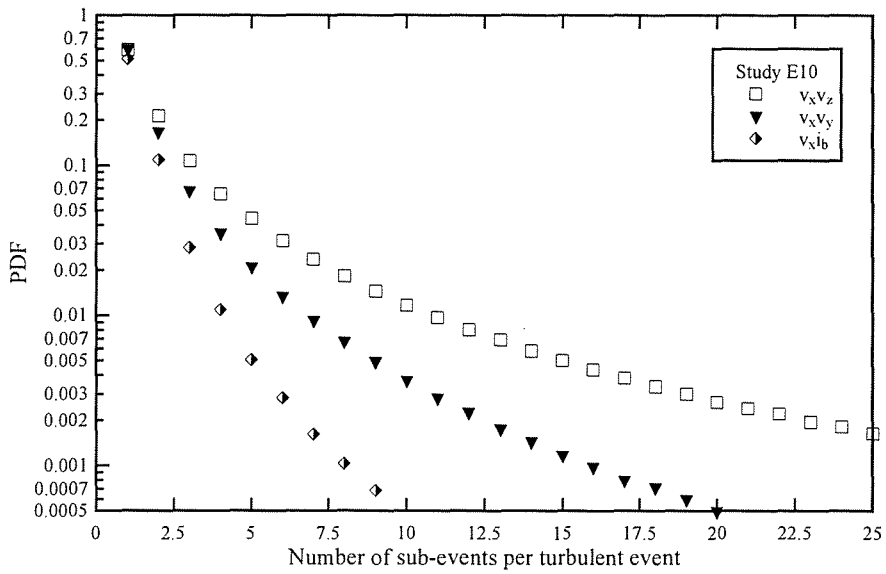

Figure 17. Normalised probability distribution function of the number of turbulent sub-events per turbulent event for the momentum flux v_xv_z, v_xv_y and v_xi_b - Data collected at z = 0.38 m (ADV2 unit) for the entire field study E10 (Eprapah Creek, Australia).

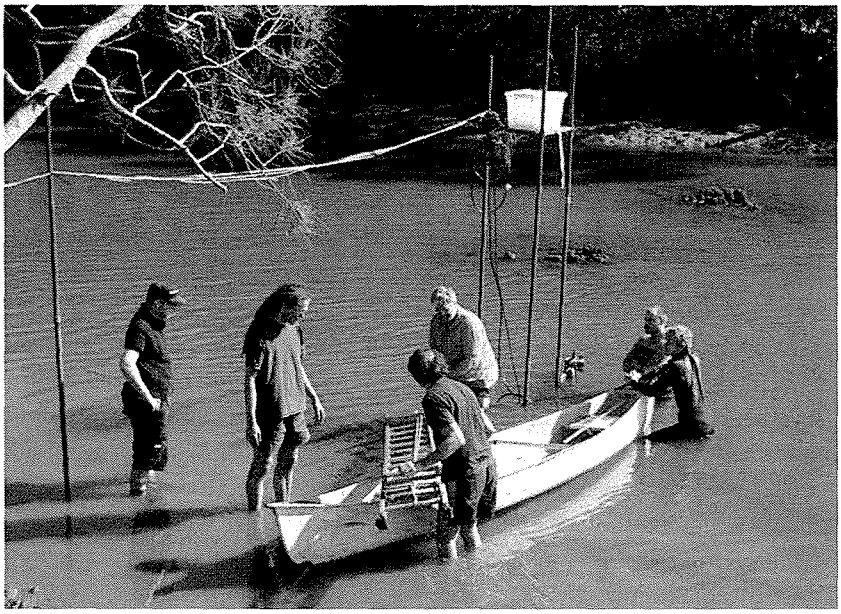

(A) Field work in a small estuary in Australia (Eprapah Creek) at low tide (study E10) (Courtesy of Dr S. FURUYAMA).

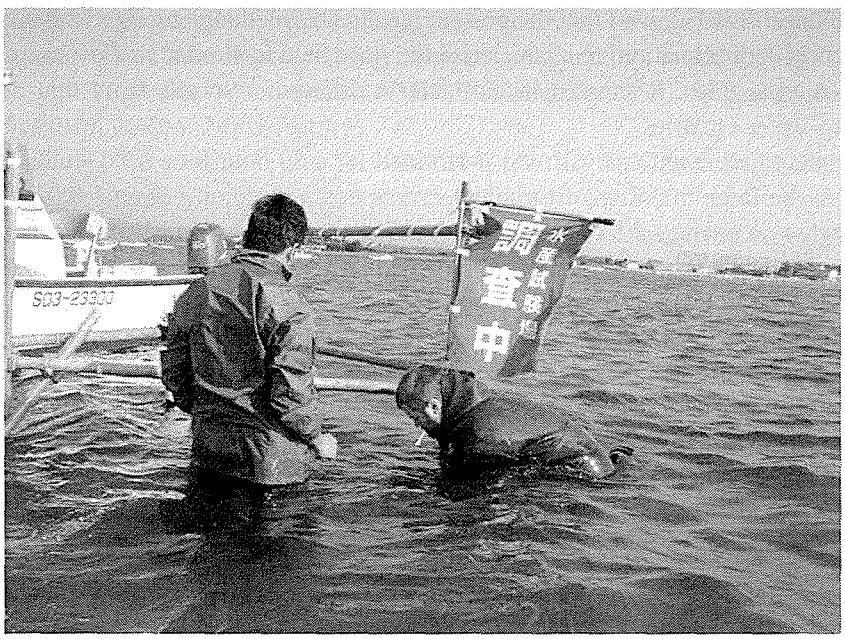

(B) Field work in a shallow-water saltwater lake in Japan (Hamana Lake) in December 2005 (Courtesy of Professor S. AOKI).

Figure 18. Field measurements in shallow water estuaries.

5. CONCLUSION

In small estuaries, the predictions of scalar dispersion can rarely be estimated accurately because of a lack of fundamental understanding of the turbulence structure. Detailed turbulent velocity and suspended sediment concentration measurements were performed simultaneously and continuously at high frequency for between 25 and 50 hours per investigation in shallow-water estuaries with semi-diurnal tides in Australia and Japan (Fig. 18). The detailed analyses provided a unique characterisation of the turbulent mixing processes and suspended sediment fluxes.

Continuous turbulent velocity sampling at high frequency allowed a detailed characterisation of the turbulence field in estuarine systems and its variations during the tidal cycle. The turbulence was neither homogeneous nor isotropic. It was not a purely Gaussian process, and the small departures from Gaussian probability distribution were an important feature of the turbulent processes. A striking feature of the present data sets was the large and rapid fluctuations in all turbulence characteristics and of the suspended sediment fluxes during the tidal cycles. This was rarely documented, but an important characteristic of the newer data sets is the continuous high frequency sampling over relatively long periods. The findings showed that the turbulent properties, and integral time and length scales should not be assumed constant in a shallow estuary. The integral time scales for turbulence and suspended sediment concentration were similar during flood tides, but differed significantly during ebb tides. It is believed that the present results provided a picture general enough to be used, as a first approximation, to characterise the flow field in similar shallow-water estuaries with semi-diurnal tides. It showed in particular a different response from that observed in larger, deep-water estuaries.

A turbulent flux event analysis was performed for a 50 hour long field study. The results showed that the large majority of turbulent events had a duration between 0.04 s and 0.3 s, and there were on average 1 to 4 turbulent events per second. A number of turbulent bursting events consisted of consecutive sub-events, with between 1 and 3 sub-events per event on average for all turbulent fluxes. A comparison with atmospheric boundary layer results illustrated a number of similarities between the two types of turbulent flows. Both studies implied that the amplitude of an event and its duration were nearly independent.

Overall the present research highlighted some turbulent processes that were rarely documented in previous studies. However, an important feature of the present analysis was the continuous high frequency sampling data sets collected during relatively long periods, as well as the simultaneous sampling of both turbulent velocities and suspended sediment concentrations.

ACKNOWLEDGMENTS

The writers acknowledge the assistance of and inputs from Prof. Shin-ichi AOKI (Toyohashi University of Technology), Dr Richard BROWN (Q.U.T.), John FERRIS (Queensland E.P.A.), and Dr Ian RAMSAY (Queensland E.P.A.). They acknowledge further the contribution of the numerous people involved in the field works.

REFERENCES

[1] Bauer B.O., Yi, J., Namikas, S.L, and Sherman, D.J. (1998). "Event Detection and Conditional Averaging in Unsteady Aeolian Systems." *Jl of Arid Env.*, Vol. 39, pp. 345-375.

[2] Bowden, K.F., and Ferguson, S.R. (1980). "Variations with Height of the Turbulence in a Tidally-Induced Botom Boundary Layer." *Marine Turbulence*, J.C.J. NIHOUL, Ed., Elsevier, Amsterdam, The Netherlands, pp. 259-286.

[3] Bowden, K.F. and Howe, M.R. (1963). "Observations of turbulence in a tidal current." *Journal of Fluid Mechanics*, Vol. 17, No. 2, pp. 271-284.

[4] Bradshaw, P. (1971). "An Introduction to Turbulence and its Measurement." *Pergamon Press*, Oxford, UK, The Commonwealth and International Library of Science and technology Engineering and Liberal Studies, Thermodynamics and Fluid Mechanics Division, 218 pages.

[5] Chanson, H. (2003). "A Hydraulic, Environmental and Ecological Assessment of a Sub-tropical Stream in Eastern Australia: Eprapah Creek, Victoria Point QLD on 4 April 2003." *Report No. CH52/03*, Dept. of Civil Engineering, The University of Queensland, Brisbane, Australia, June, 189 pages.

[6] Chanson, H. (2004). "Environmental Hydraulics of Open Channel Flows." *Elsevier Butterworth-Heinemann*, Oxford, UK, 483 pages.

[7] Chanson, H., Brown, R., Ferris, J., Ramsay, I., and Warburton, K. (2005). "Preliminary Measurements of Turbulence and Environmental Parameters in a Sub-Tropical Estuary of Eastern Australia." *Environmental Fluid Mechanics*, Vol. 5, No. 6, pp. 553-575 (DOI: 10.1007/s10652-005-0928-y).

[8] Chanson, H., Takeuchi, M., and Trevethan, M. (2008a). "Using Turbidity and Acoustic Backscatter Intensity as Surrogate Measures of Suspended Sediment Concentration in a Small Sub-Tropical Estuary." *Journal of Environmental Management*, Vol. 88, No. 4, Sept., pp. 1406-1416 (DOI: 10.1016/j.jenvman.2007.07.009).

[9] Chanson, H., Trevethan, M., and Aoki, S. (2008b). "Acoustic Doppler Velocimetry (ADV) in Small Estuary : Field Experience and Signal Post-Processing." *Flow Measurement and Instrumentation*, Vol. 19, No. 5, pp. 307-313 (DOI: 10.1016/j.flowmeasinst.2008.03.003).

[10] Digby, M.J., Saenger, P., Whelan, M.B., Mcconchie, D., Eyre, B., Holmes, N., Bucher, D. (1999). "A Physical Classification of Australian Estuaries." *Report No. 9*, LWRRDC, Australia, National River Health Program, Urban sub-program, Occasional Paper, 16/99.

[11] Dyer, K.R. (1997). "Estuaries. A Physical Introduction." *John Wiley*, New York, USA, 2nd edition, 195 pages.

[12] Finnigan, J. (2000). "Turbulence in Plant Canopies." *Ann. Rev. Fluid Mech.*, Vol. 32, pp. 519-571.

[13] Fransson, J.H.M., Matsubara, M., and Alfredsson, P.H. (2005)." Transition Induced by Free-stream Turbulence." *Jl of Fluid Mech.*, Vol. 527, pp. 1-25.

[14] Fugate, D.C., and Friedrichs, C.T. (2002). "Determining Concentration and Fall Velocity of Estuarine Particle Populations using ADV, OBS and LISST." *Continental Shelf Research*, Vol. 22, pp. 1867-1886.

[15] Hallback, M., Groth, J., and Johansson, A.V. (1989). "A Reynolds Stress Closure for the Dissipation in Anisotropic Turbulent Flows." *Proc. 7th Symp. Turbulent Shear Flows*, Stanford University, USA, Vol. 2, pp. 17.2.1-17.2.6.

[16] Ham, R. van der, Fromtijn, H.L., Kranenburg, C., and Winterwerp, J.C. (2001). "Turbulent Exchange of Fine Sediments in a Tidal Channel in the Ems/Dollard Estuary. Part I: Turbulence Measurements." *Continental Shelf Research*, Vol. 21, pp. 1605-1628.

[17] Hinterberger, C., Fröhlich, J., and Rodi, W. (2008). "2D and 3D Turbulent Fluctuations in Open Channel Flow with Re_τ = 590 studied by Large Eddy Simulation." *Flow Turbulence Combustion*, Vol. 80, No. 2, pp. 225-253 (DOI: 10.1007/s10494-007-9122-2).

[18] Hinze, J.O. (1975). "Turbulence." *McGraw-Hill Publ.*, 2nd Edition, New York, USA.

[19] Hossain, S., Eyre, B., and Mcconchie, D. (2001). "Suspended Sediment Transport Dynamics in the Subtropical Micro-tidal Richmond River Estuary, Australia." *Estuarine, Coastal and Shelf Science*, Vol. 52, pp. 529–541.

[20] Johansson, A.V., and Alfredsson, P.H. (1982). "On the Structure of Turbulent Channel Flow." *Jl of Fluid Mech.*, Vol. 122, pp. 295-314.

[21] Kawanisi, K., and Yokosi, S. (1994). "Mean and Turbulence Characteristics in a Tidal River." *Continental Shelf Research*, Vol. 17, No. 8, pp. 859-875.

[22] Kawanisi, K., Tsutsui, T., Nakamura, S., and Nishimaki, H. (2006). "Influence of Tidal Range and River Discharge on Transport of Suspended Sediment in the Ohta Floodway." *Jl of Hydroscience and Hyd. Eng.*, JSCE, Vol. 24, No. 1, May, pp. 1-9.

[23] Kline, S.J., Reynolds, W.C., Schraub, F.A. and Runstaller, P.W. (1967)."The structure of turbulent boundary layers." Journal of Fluid Mechanics, Vol. 30, No. 4, pp. 741-773.

[24] Koch, C., and Chanson, H. (2005). "An Experimental Study of Tidal Bores and Positive Surges: Hydrodynamics and Turbulence of the Bore Front." *Report No. CH56/05*, Dept. of Civil Engineering, The University of Queensland, Brisbane, Australia, July, 170 pages.

[25] Larcombes, P. and Ridd, P.V. (1992). "Dry Season Hydrodynamics and Sediment Transport in a Mangrove Creek." *Proceedings 6th International Biennial Conf on Physics of Estuaries and Coastal Seas*, Margaret River WA, Australia, Paper 23. (Also *Mixing in Estuaries and Coastal Seas*, Coastal and Estuarine Studies Vol. 50, AGU, New York, USA, 1996, pp. 388-404.)

[26] Montes, J.S. (1998). "Hydraulics of Open Channel Flow." *ASCE Press*, New-York, USA, 697 pages.

[27] Narasimha, R., Kumar, S.R., Prabhu, A., and Kailas, S.V. (2007). "Turbulent Flux Events in a Nearly Neutral Atmospheric Boundary Layer." *Phil. Trans. Royal Soc., Series A*, Vol. 365, pp. 841-858.

[28] Nezu, I. (2005). "Open-Channel Flow Turbulence and its Research prospect in the 21st Century." *Jl of Hyd. Engrg.*, ASCE, Vol. 131, No. 4, pp. 229-246.

[29] Nezu, I., and Nakagawa, H. (1993). "Turbulence in Open-Channel Flows." *IAHR Monograph*, IAHR Fluid Mechanics Section, Balkema Publ., Rotterdam, The Netherlands, 281 pages.

[30] Niederschulte, M.A. (1989). "Turbulent Flow Through a Rectangular Channel." *Ph.D. thesis*, Dept. of Chem. Eng., University of Illinois, Urbana-Champaign, USA, 417 pages.

[31] Nielsen, P. (1992). "Coastal Bottom Boundary Layers and Sediment Transport." *Advanced Series on Ocean Eng.*, Vol. 4, World Scientific Publ., Singapore.

[32] Nikora, V., Goring, D., and Ross, A. (2002). "The Structure and Dynamics of the Thin Near-Bed Layer in a Complex Marine Environment: A Case Study in Beatrix Bay, New Zealand." *Estuarine, Coastal and Shelf Science*, Vol. 54, pp. 915-926.

[33] Osonphasop, C. (1983). "The Measurements of Turbulence in Tidal Currents." *Ph.D. thesis*, Dept of Mech. Eng., Monash Univ., Australia.

[34] Osterlund, J.M., Lindgren, B., and Johansson, A.V. (2003). "Flow Structures in Zero Pressure-Gradient Turbulent Boundary Layers at High Reynolds Numbers." *Eur. Jl Mechanics B. Fluids*, Vol. 22, pp. 379-390 (DOI: 10.1016/S0997-7546(03)00034-7).

[35] Piquet, J. (1999). "Turbulent Flows. Models and Physics." *Springer*, Berlin, Germany, 761 pages.

[36] Rao, K.N., Narasimha, R., and Narayanan, A.A.B. (1971). "The "Bursting" Phenomena in a Turbulent Boundary Layer." *Jl of Fluid Mech.*, Vol. 48, Part 2, pp. 339-352.

[37] Reynolds, O. (1883). "An Experimental Investigation of the Circumstances which Determine whether the Motion of Water shall be Direct or Sinuous, and the Laws of Resistance in Parallel Channels." *Phil. Trans. Roy. Soc. Lond.*, Vol. 174, pp. 935-982.

[38] Reynolds, O. (1887) "On Certain Laws Relating to the Regime of Rivers and Estuaries, and on the Possibility of Experiments on a Small Scale." *British Association Report*, UK.

[39] Rudra Kumar, S., Ameenulla, S., and Prabhu, A. (1995). "MONTBLEX Tower Observations: Instrumentation, Data Acquisition and Data Quality." *Proc. Indian Acad. Science (Earth Planet Science)*, Vol. 104, No. 2, pp. 221-248.

[40] Savenije, H.H.G. (2005). "Salinity and Tides in Alluvial Estuaries." *Elsevier*, Amsterdam, The Netherlands, 194 pages.

[41] Schlichting, H. (1979). "Boundary Layer Theory." *McGraw-Hill*, New York, USA, 7th edition.

[42] Shiono, K., and West, J.R. (1987). "Turbulent Perturbations of Velocity in the Conwy Estuary." *Estuarine, Coastal and Shelf Science*, Vol. 25, pp. 533-553.

[43] Tachie, M.F. (2001). "Open Channel Turbulent Boundary Layers and wall Jets on Rough Surfaces." *Ph.D. thesis*, Dept. of Mech. Eng., Univers. of Saskatchewan, Canada, 238 pages.

[44] Thorne, P.D., Vincent, C.E., Hardcastle, P.J., Rehman, S., and Pearson, N. (1991). "Measuring Suspended Sediment Concentrations using Backscatter Devices." *Marine Geology*, Vol. 98, pp. 7-16.

[45] Trevethan, M. (2008). "A Fundamental Study of Turbulence and Turbulent Mixing in a Small Subtropical Estuary." *Ph.D. thesis*, Div. of Civil Engineering, The University of Queensland, 342 pages.

[46] Trevethan, M., Chanson, H., and Takeuchi, M. (2007a). "Continuous High-Frequency Turbulence and Sediment Concentration Measurements in an Upper Estuary." *Estuarine Coastal and Shelf Science*, Vol. 73, No. 1-2, pp. 341-350 (DOI:10.1016/j.ecss.2007.01.014).

[47] Trevethan, M., Chanson, H., and Brown, R.J. (2007b). "Turbulence and Turbulent Flux Events in a Small Subtropical Estuary." *Report No. CH65/07*, Hydraulic Model Report series, Div. of Civil Engineering, The University of Queensland, Brisbane, Australia, November, 67 pages.

[48] Trevethan, M., Chanson, H., and Brown, R. (2008). "Turbulence Characteristics of a Small Subtropical Estuary during and after some Moderate Rainfall." *Estuarine Coastal and Shelf Science*, Vol. 79, No. 4, pp. 661-670 (DOI: 10.1016/j.ecss.2008.06.006).

[49] Voulgaris, G., and Meyers, S.T. (2004). "Temporal Variability of Hydrodynamics, Sediment Concentration and Sediment Settling in a Tidal Creek." *Continental Shelf Research*, Vol. 24, pp. 1659-1683.

[50] West, J.R. and Oduyemi, K.O.K. (1989). "Turbulence measurements of suspended solids concentration in estuaries." *Journal of Hydraulic Engineering*, ASCE, Vol. 115, No. 4, pp. 457-473.

[51] Xie, Q. (1998). "Turbulent Flows in Non-Uniform Open Channels : Experimental Measurements and Numerical Modelling." *Ph.D. thesis*, Dept. of Civil Eng., University Of Queensland, Australia, 339 pages.

INTERNET REFERENCES

A Hydraulic, Environmental and Ecological Assessment of a Sub-tropical Stream in Eastern Australia: Eprapah Creek, Victoria Point QLD on 4 April 2003	{http://www.uq.edu.au/~e2hchans/eprapa.html}
Queensland EPA water quality monitoring	{http://www.epa.qld.gov.au/environmental_management/water/water_quality_monitoring/}
Eprapah Creek Catchment Landcare Association Inc. (ECCLA)	{http://eprapah.scouting.net.au/index/projects/landcare.htm}
Research publications in hydraulic engineering and applied fluid mechanics	{http://espace.library.uq.edu.au/list/author_id/193/}

OPEN ACCESS REPOSITORIES

OAIster	{http://www.oaister.org/}
UQeSpace	{http://espace.library.uq.edu.au/}

Reviewed by Professor Michele MOSSA, Politecnico di Bari (Italy)